Supporting Information for

Inactivation of Multiple Bacterial Histidine Kinases by Targeting the ATP-Binding Domain

Kaelyn E. Wilke,[†] Samson Francis,[†] and Erin E. Carlson*[,†,‡]

[†]Department of Chemistry, Indiana University, 800 E. Kirkwood Ave., Bloomington, IN 47405
[‡]Department of Molecular and Cellular Biochemistry, Indiana University, 212 S. Hawthorne Drive, Bloomington, IN 47405
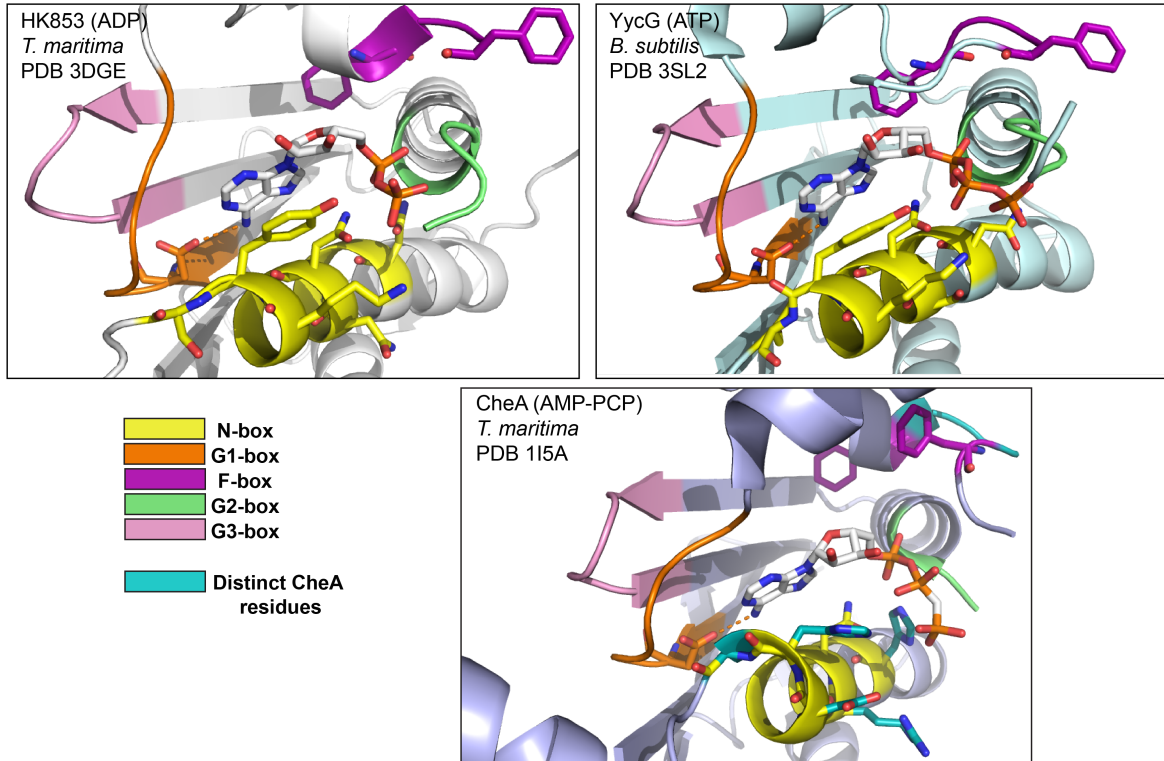
*To whom correspondence should be addressed. E-mail: carlsone@umn.edu

Supporting Information Table of Contents   **Page**

1. List of Figures

2. Supplementary Figures

HK853 (ADP)
T. maritima
PDB 3DGE

YycG (ATP)
B. subtilis
PDB 3SL2

CheA (AMP-PCP)
T. maritima
PDB 1I5A

- N-box
- G1-box
- F-box
- G2-box
- G3-box

- Distinct CheA residues

```
HK853 (T. maritima)   324  REKVDLCDLVESAVNAIKEFASSHNVNVLFESNVPCPVEAYIDPTRIRQVLLNLLNNGVK  383
VICK  (S. pneumoniae) 323  ------------------------------------------IDTDKMTQVVDNILNNAIK  341
CHEA  (E. coli)       369  ------------------------------------------RIIDPLTHLVRNSLD  383

HK853 (T. maritima)   384  YSKKDAPD----------KYVKVILDEKDGGVLIIVEDNGIGIP----------------  417
VICK  (S. pneumoniae) 342  YS----PDG---------GKITVRMKTTEDQMILSISDHGLGIP----------------  372
CHEA  (E. coli)       384  HGI-ELPEKRLAAGKNSVGNLILSAEHQGGNICIEVTDDGAGLNRERILAKAASQGLTVS  442

HK853 (T. maritima)   418  -----DHAKDRIFEQ-FYRVDSSLTYEVPGTGLGLAITKEIVELHGGRIWVESEVGKGSR  471
VICK  (S. pneumoniae) 373  -----KQDLPRIFDR-FYRVDRARSRAQGGTGLGLSIAKEIIKQHKGFIWAKSEYGKGST  426
CHEA  (E. coli)       443  ENMSDDEVAMLIFAPGFSTAEQVT--DVSGRGVGMDVVKRNIQKMGGHVEIQSKQGTGTT  500

HK853 (T. maritima)   472  FFVWIPKDRA  481
VICK  (S. pneumoniae) 427  FTIVLPYDK-  435
CHEA  (E. coli)       501  IRILLPLTL-  509
```

Figure S1. Conservation among HKs used in experiments. Using the sequences of our protein constructs, the ATP-binding domains were confirmed using "HATPase_c" in the SMART database (http://smart.embl-heidelberg.de/). ATP-binding domain sequences were aligned using the Cobalt: Multiple Alignment Tool (NCBI). Homology boxes are designated through shading of both sequences and structures. Because structures were not available for VicK (*S. pneumoniae*) and CheA (*E. coli*), homologous proteins with structural data were used for

viewing the ATP-binding domains (YycG of *B. subtilis* and CheA of *T. maritima*, respectively). Important residues for substrate binding are shown in stick form. Teal-colored amino acids represent distinct differences in CheA (class-9 HKs) from class-1 HK853 and VicK and HKs at large. It is for this diversity that CheA was included as a protein in follow-up screening. ATP lids were removed for easier viewing. Structural images were prepared in PyMOL, and homology boxes were assigned based on assignments in the literature.(*1–4*)
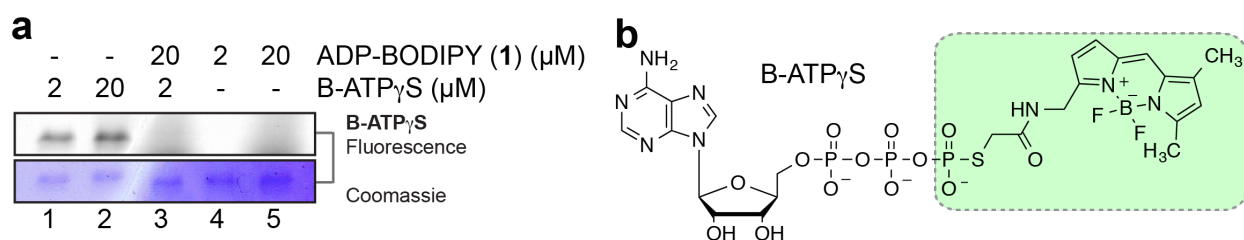
Figure S2. ADP-BODIPY (**1**) competes with activity-based probe, BODIPY-FL-ATPγS (B-ATPγS). a) Sodium dodecyl sulfate-polyacrylamide gel electrophoresis (SDS-PAGE) gel lanes 1 and 2 show labeling of HK853 with 2 and 20 µM B-ATPγS, which is inhibited when 10-fold ADP-BODIPY is added (lane 3). Since ADP-BODIPY (**1**) is a nonhydrolyzable nucleotide analogue, no fluorescent band should be observed in lanes 3, 4, and 5. This gel confirmed that there was no probe turnover and that ADP-BODIPY (**1**) binds specifically to HK. b) B-ATPγS activity-based probe, highlighting the portion of the probe that autothiophosphorylates HK853.(*5*)
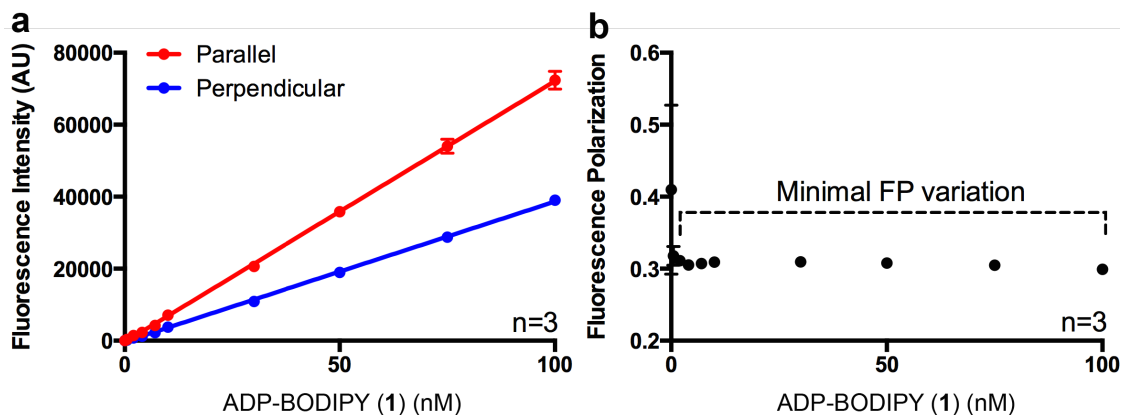
Figure S3. Fluorescence polarization (FP) probe invariability. a) Parallel and perpendicular fluorescence intensities (FIs) when 25 μM HK853 is mixed with increasing concentrations of ADP-BODIPY (**1**). As expected, FIs are linear with ADP-BODIPY (**1**) concentration. b) Calculated FP from FIs in panel a, showing that FP remains constant from 0.01−100 nM ADP-BODIPY (**1**). Signal becomes noisy below 10 nM as the limit of detection of the microplate reader is approached.
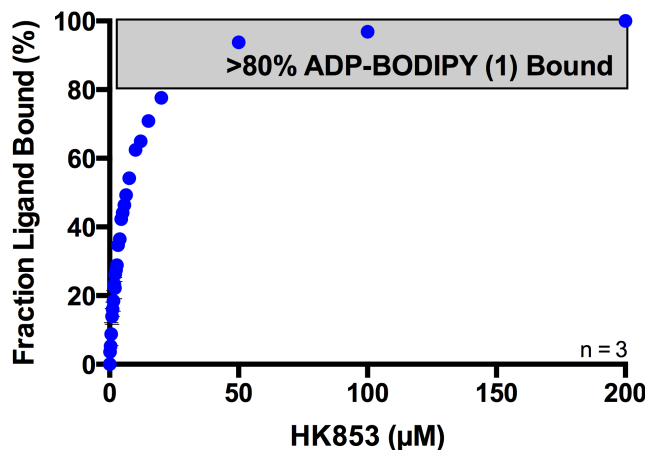
Figure S4. Fraction ADP-BODIPY (**1**) bound with increasing HK853. The gray box illustrates HK853 concentrations at which >80% of 10 nM ADP-BODIPY (**1**) is bound. As a result, 25 μM HK853 was used to provide an ample signal window for detecting probe displacement.
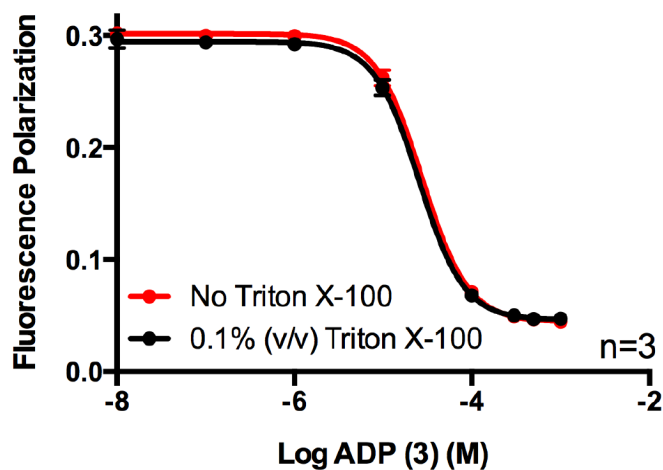
Figure S5. FP assay tolerance to Triton X-100. Adenosine diphosphate (ADP) dose-response displacement of 10 nM ADP-BODIPY (**1**) from 25 μM HK853 in the absence and presence of 0.1% (v/v) Triton X-100 shows no difference in FP.
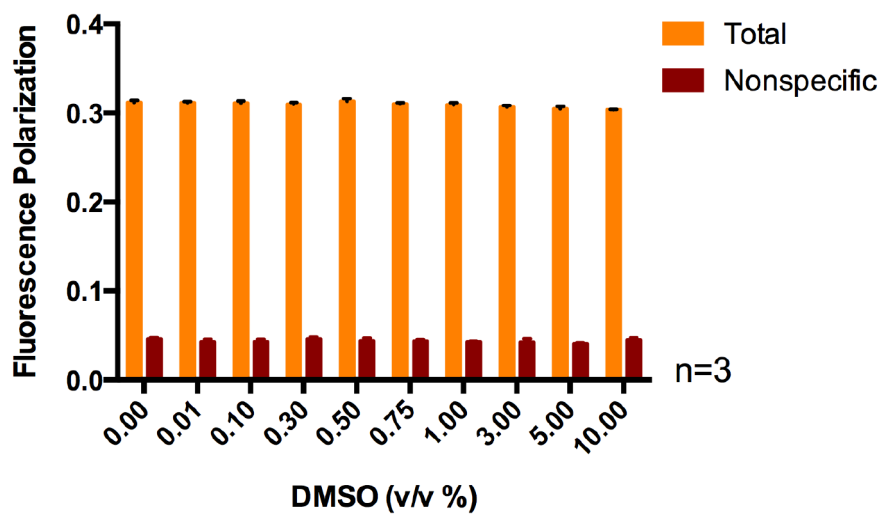
Figure S6. FP assay tolerance to dimethyl sulfoxide (DMSO). Increasing concentrations of DMSO were added to 25 μM HK853 and 10 nM ADP-BODIPY (**1**). Within the DMSO range tested, total and nonspecific FP (and therefore specific FP) are constant.
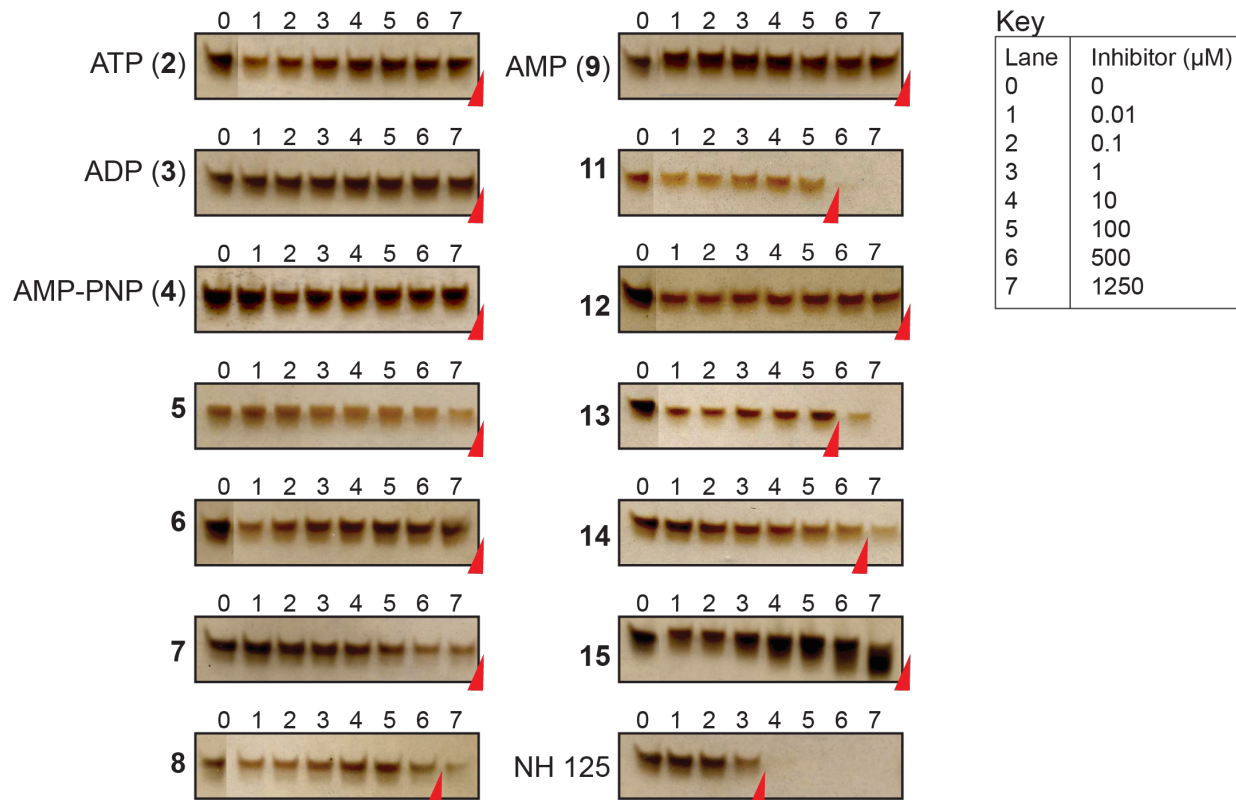
Figure S7. Representative gels from aggregation screening. Each of the 115 compounds was added at 0–1250 µM to 0.44 µM HK853 under non-denaturing conditions. Native polyacrylamide gel electrophoresis (native-PAGE) and silver staining shows "cut-off" concentrations where the HK853 dimer disappears due to aggregation (red arrow head). NH125, a compound that inhibits HK autophosphorylation through aggregation,(*6*) was used as a positive control. Because some compounds subtly aggregated with increasing concentration, Triton X-100 was added to subsequent activity assays. Compound **15** may have a denaturing effect on HK853.
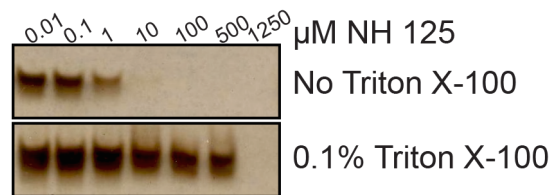
Figure S8. Triton X-100 helps prevent HK853 aggregation. The aggregator NH125 mixed with 0.44 μM HK853 under non-denaturing conditions with and without 0.1% (v/v) Triton X-100. Native-PAGE and silver staining shows that the detergent helps maintain the dimeric HK853 (except at 1.25 mM NH125). In subsequent assays, it was important that decreases in activity-based labeling were due to inhibition of the protein and not aggregation. As a result, 0.1% (v/v) Triton X-100 was added to all activity assays with our test compounds as an additive within established cut-off concentrations in Figure S7.

a) Increasing concentrations of lead compound were mixed with HK853 under denaturing conditions with and without Triton X-100. Native-PAGE and silver staining show that HK853 is not aggregated at the concentrations used in enzymatic competition assays. b) Lead compound was pre-incubated with HK proteins prior to adding B-ATPγS (HK853) or ATP[γ-^{33}P] (VicK and CheA). Fluorescence and phosphorescence shows inhibition of HK activity, and the silver-stained HK853 gel shows even protein loading. Each gel is representative of duplicate data.

Figure S9. Aggregation analysis and HK inhibition with lead **5** at 0–1250 µM.

Figure S10. Aggregation analysis and HK inhibition with lead **6** at 0–1250 µM.

Figure S11. Aggregation analysis and HK inhibition with lead **7** at 0–1250 µM.

a **AGGREGATION** (Native-PAGE)

0 0.01 0.1 1 5 10 20 50 100 200 300 400 500 µM **8**

HK853

No Triton X-100

0.1% (v/v) Triton X-100

b **ACTIVITY** (SDS-PAGE)

0 0.01 0.1 1 5 10 20 50 100 200 300 400 500 µM **8**

HK853

— **B-ATPγS** Fluorescence

— Silver stain

VicK

CheA

— ATP [γ-^{33}P] Phosphorescence

Figure S12. Aggregation analysis and HK inhibition with lead **8** at 0–500 µM.

a **AGGREGATION** (Native-PAGE)

0 0.01 0.1 1 5 10 20 50 150 500 700 1000 1250 µM ADP (**3**)

HK853

No Triton X-100

0.1% (v/v) Triton X-100

b **ACTIVITY** (SDS-PAGE)

0 0.01 0.1 1 5 10 20 50 150 500 700 1000 1250 µM ADP (**3**)

HK853

— **B-ATPγS** Fluorescence

— Silver stain

VicK

CheA

— ATP [γ-^{33}P] Phosphorescence

Figure S13. Aggregation analysis and HK inhibition with ADP (**3**) at 0–1250 µM.

Figure S14. Aggregation analysis and HK inhibition with adenosine monophosphate (AMP) (**9**) at 0–100 mM. To obtain IC_{50} values, higher concentrations of AMP were tested relative to other compounds. Because AMP was prepared as an aqueous solution, DMSO concentration was not a limitation.
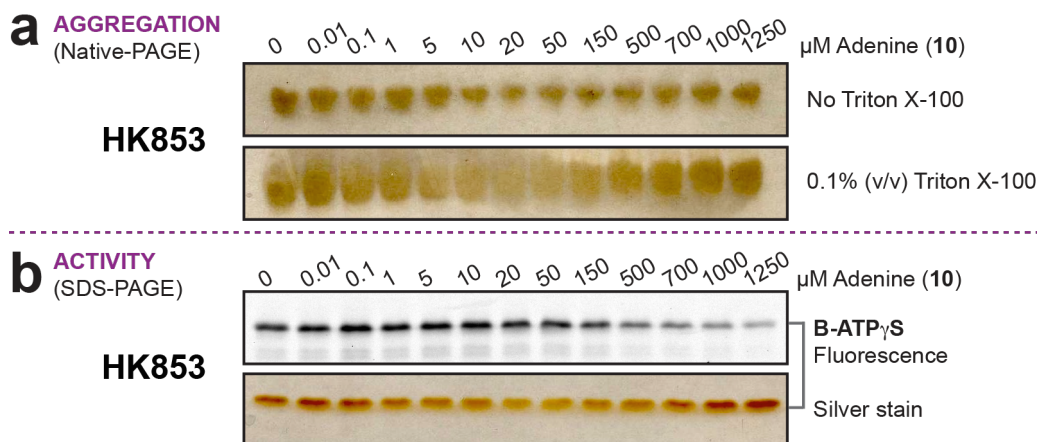
Figure S15. Aggregation analysis and HK inhibition with adenine (**10**) at 0–1250 µM.
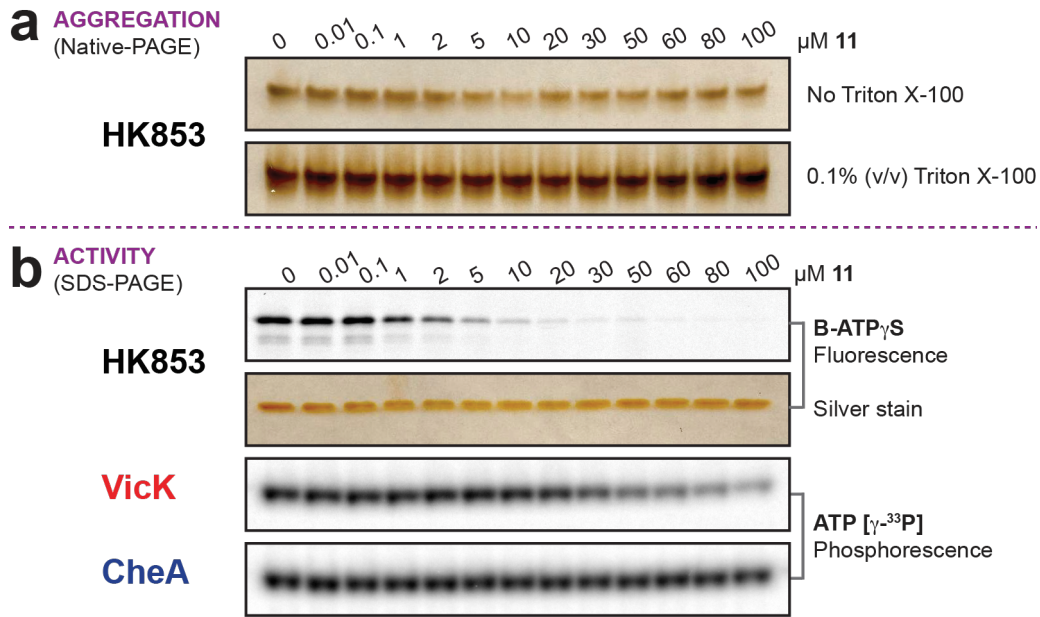
Figure S16. Aggregation analysis and HK inhibition with lead **11** at 0–100 µM.
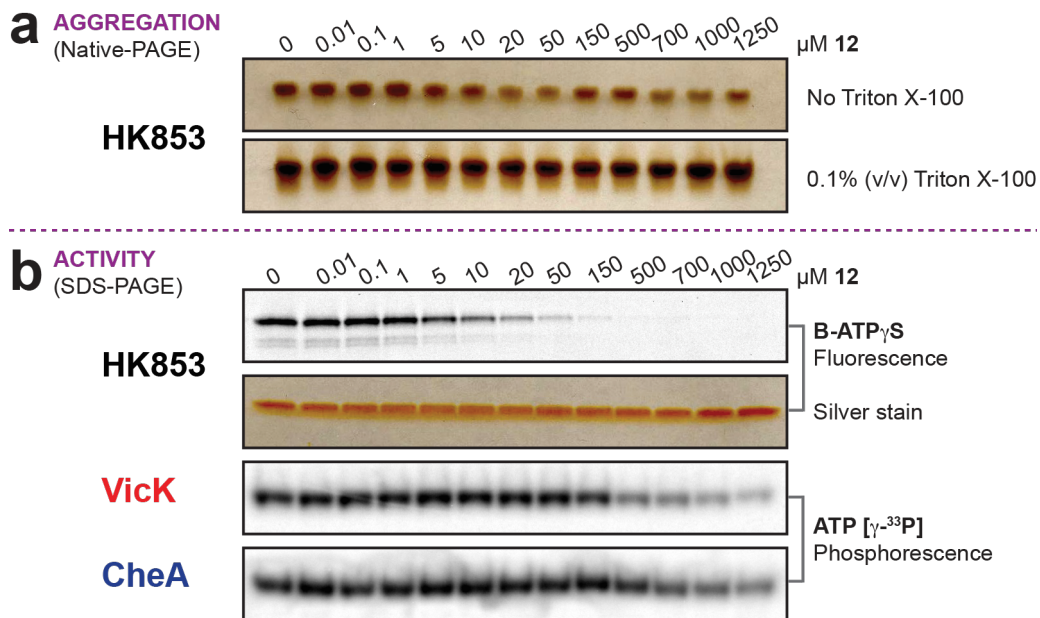
Figure S17. Aggregation analysis and HK inhibition with lead **12** at 0–1250 µM.

a AGGREGATION (Native-PAGE)

0 0.01 0.1 1 2 5 10 20 30 50 60 80 100 µM **13**

HK853

No Triton X-100

0.1% (v/v) Triton X-100

b ACTIVITY (SDS-PAGE)

0 0.01 0.1 1 2 5 10 20 30 50 60 80 100 µM **13**

HK853

B-ATPγS Fluorescence

Silver stain

VicK

CheA

ATP [γ-^{33}P] Phosphorescence
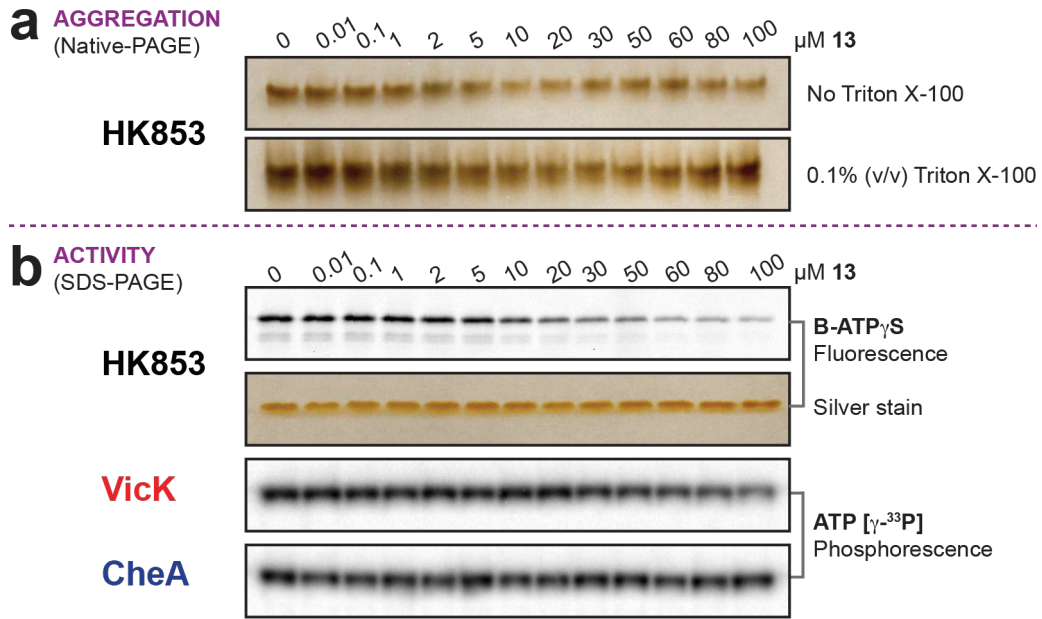
Figure S18. Aggregation analysis and HK inhibition with lead **13** at 0–100 µM.

a AGGREGATION (Native-PAGE)

0 0.01 0.1 1 5 10 20 50 100 200 300 400 500 µM **14**

HK853

No Triton X-100

0.1% (v/v) Triton X-100

b ACTIVITY (SDS-PAGE)

0 0.01 0.1 1 5 10 20 50 100 200 300 400 500 µM **14**

HK853

B-ATPγS Fluorescence

Silver stain

VicK

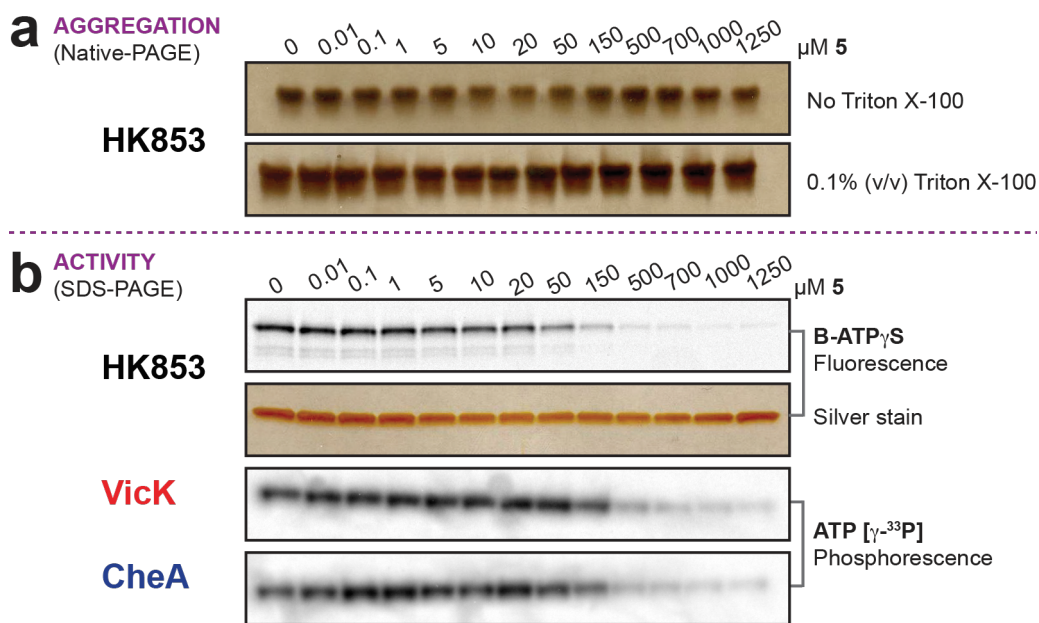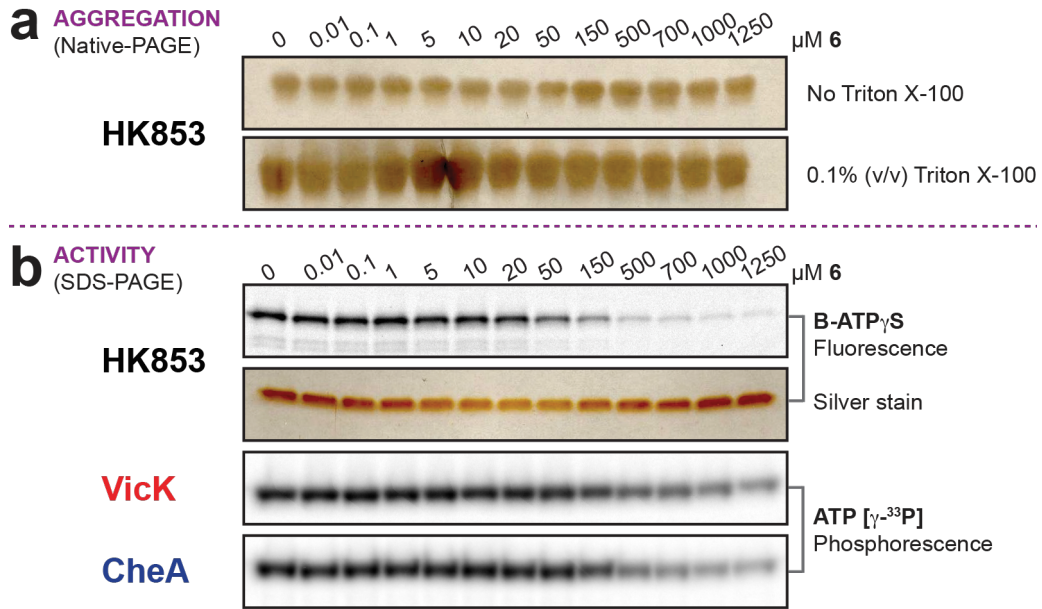**CheA**

ATP [γ-^{33}P] Phosphorescence
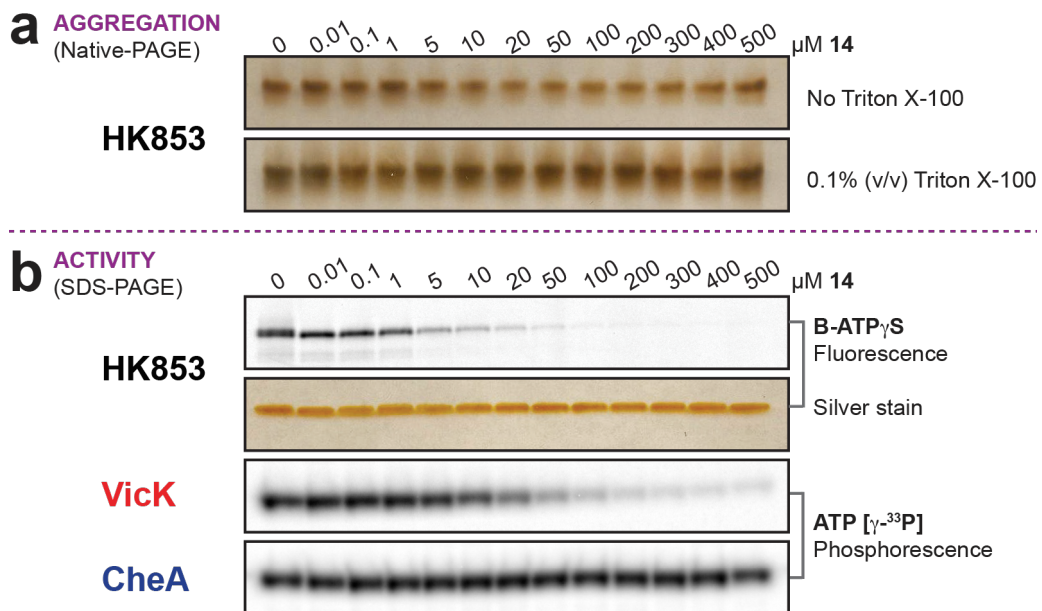
Figure S19. Aggregation analysis and HK inhibition with lead **14** at 0–500 µM.

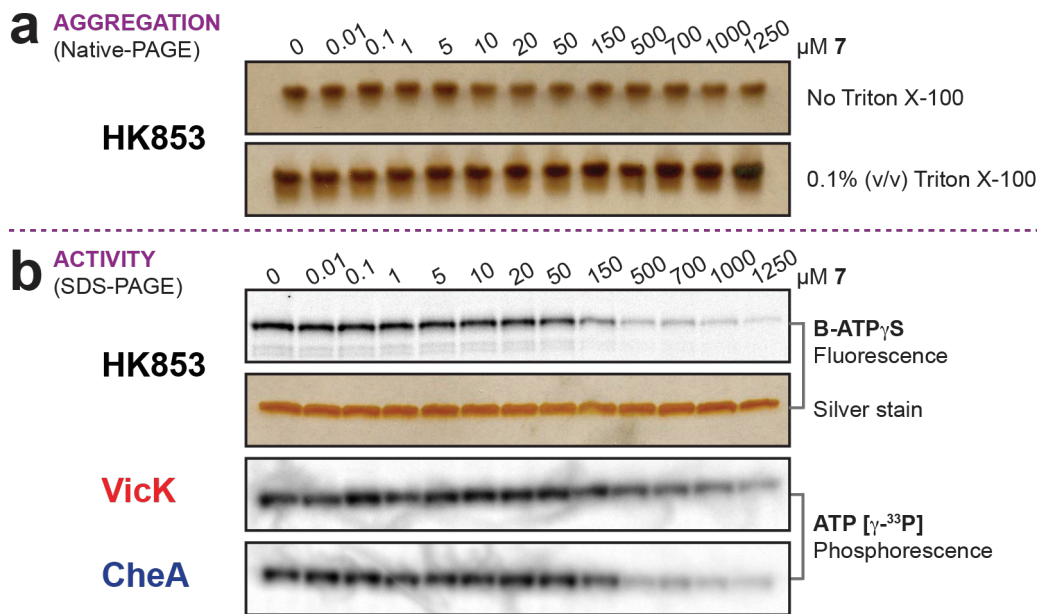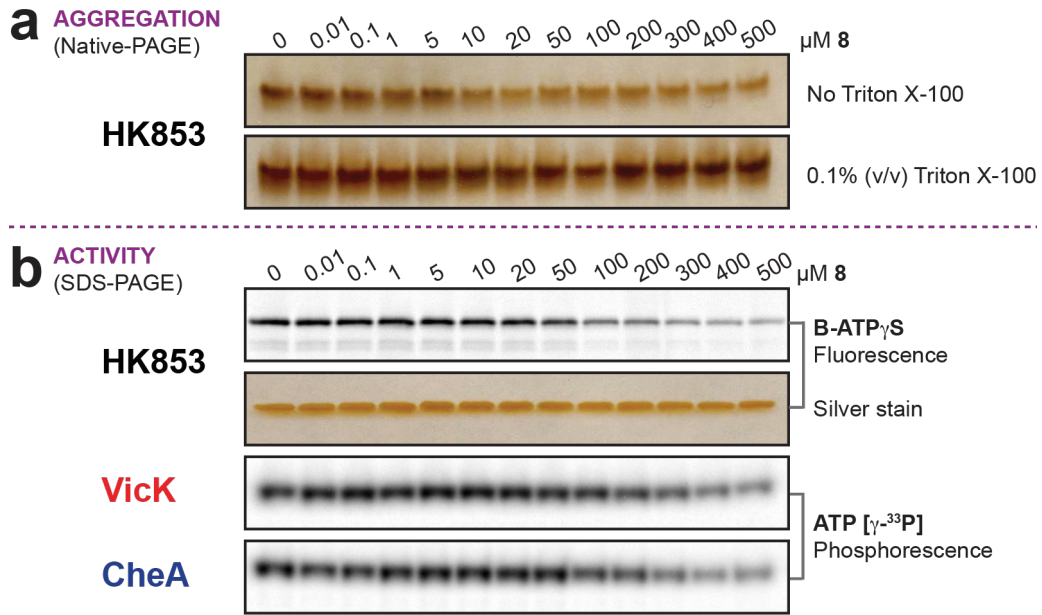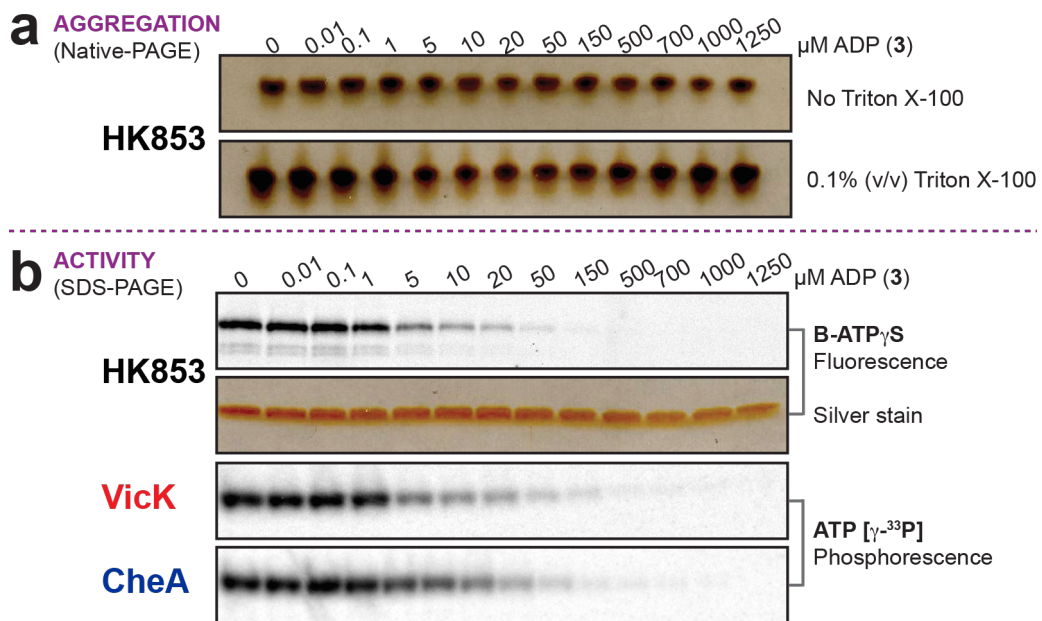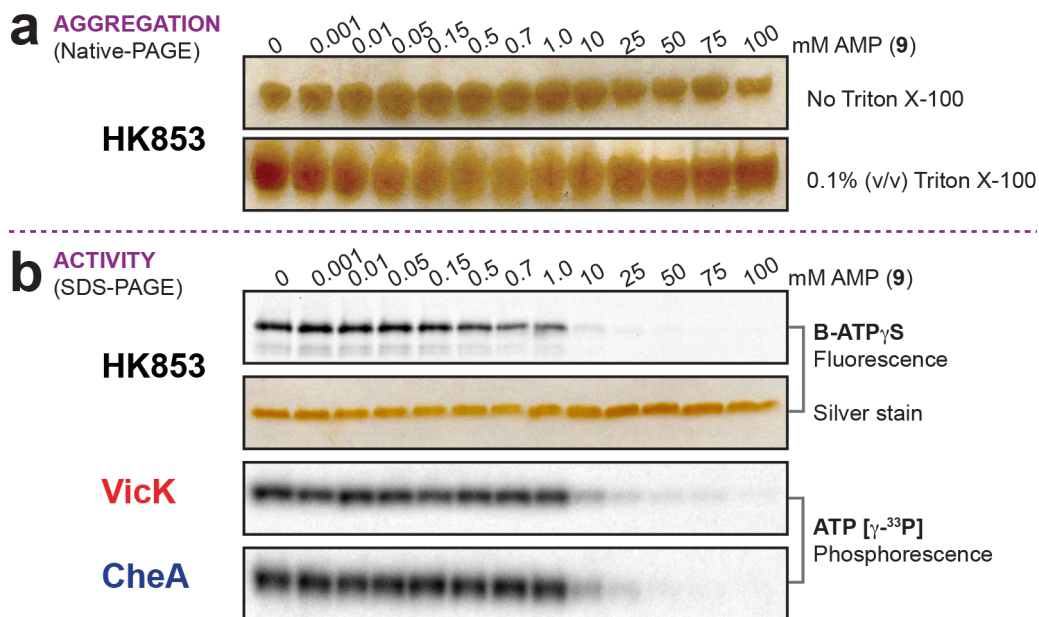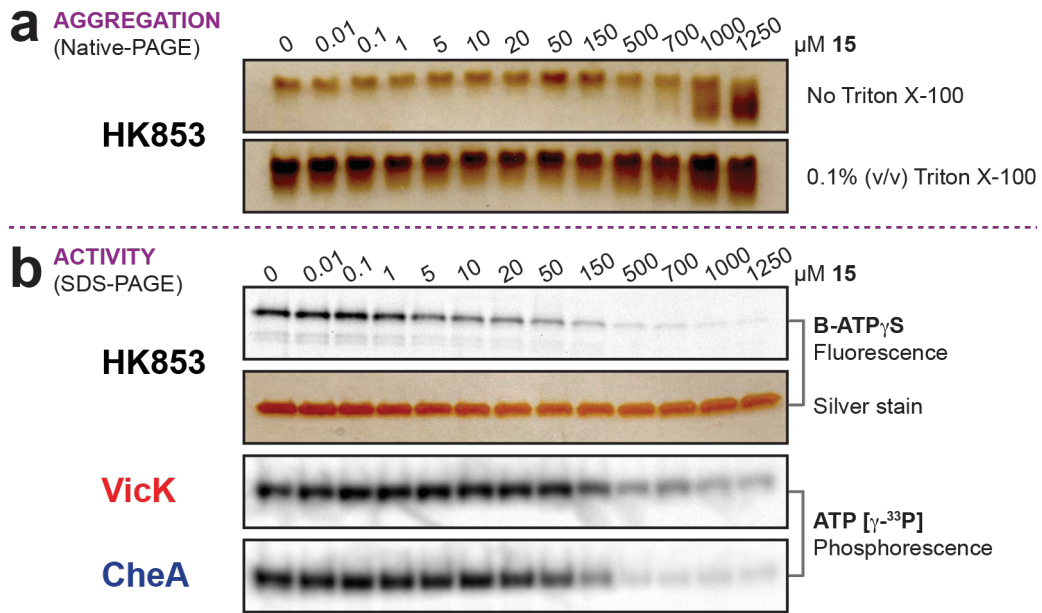**Figure S20.** Aggregation analysis and HK inhibition with lead **15** at 0–1250 µM. As seen in the final two lanes, **15** may have a denaturing effect on HK853. However, it inhibits activity where this effect is not prominent.
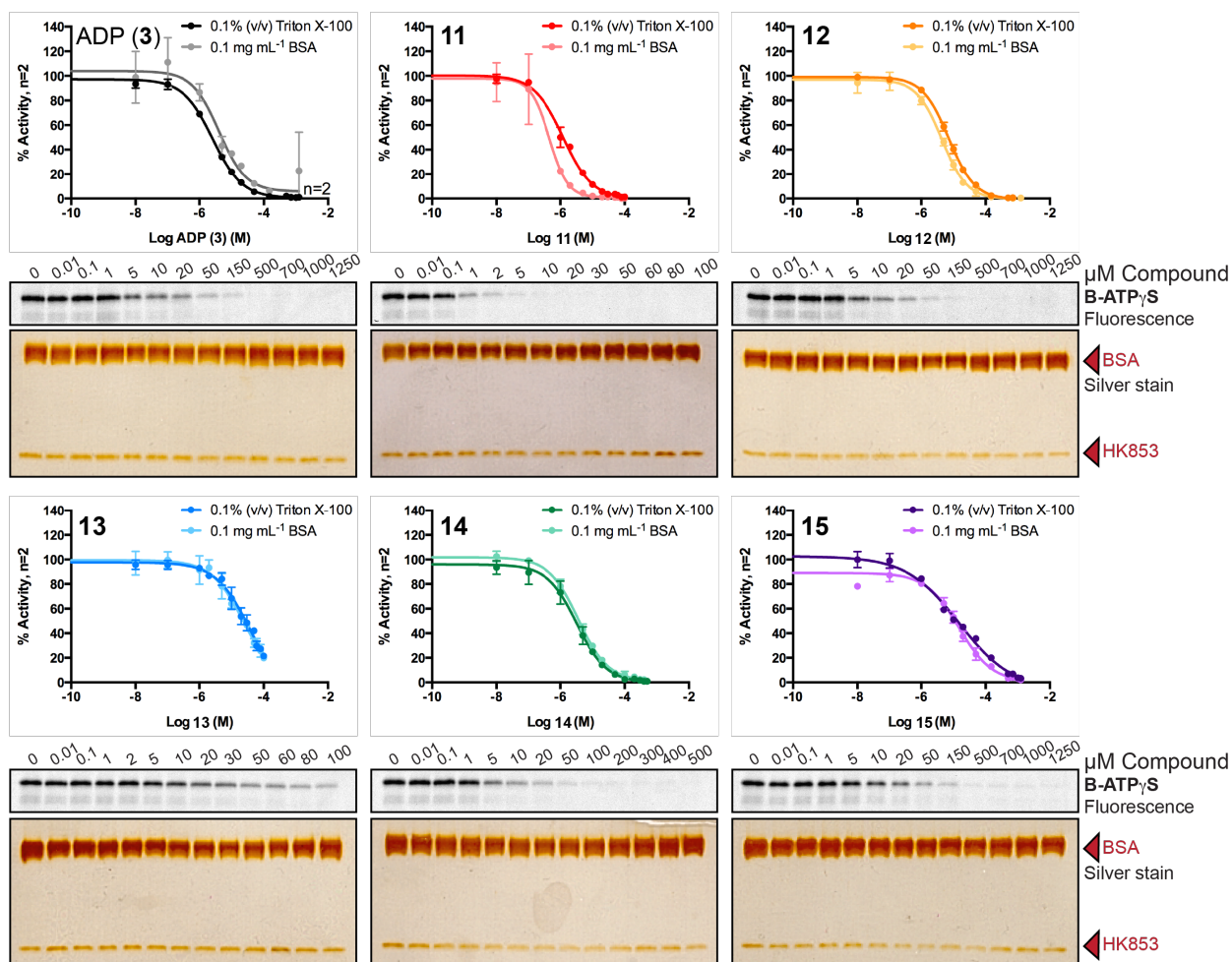
Figure S21. Bovine serum albumin (BSA) added to competition assays. B-ATPγS competition assays with HK853 were repeated for ADP (**3**) and leads **11**–**15** in the presence of 0.1 mg mL^{-1} BSA (with no detergent). DRCs were overlaid with those previously acquired using 0.1% (v/v) Triton X-100 (Figure S13, S16–S20). Silver staining shows the seven-fold greater abundance of BSA, yet the inhibition of HK853 by leads was the same. Lead **11** actually has increased activity when BSA is added. Each gel is representative of duplicate data.

Compound		1	2	3	4	5	6	7	8	9	10	11	12
DMSO (% v/v)	A	20	10	5	2.5	1.25	0.63	0.31	0.16	-	-	GC	SC
Penicillin G (µg mL^{-1})	B	32	16	8	4	2	1	0.5	0.25	0.13	0.06	GC	SC
Chloramphenicol (µg mL^{-1})	C	32	16	8	4	2	1	0.5	0.25	0.13	0.06	GC	SC
11 (µg mL^{-1})	D	128	64	32	16	8	4	2	1	0.5	0.25	GC	SC
13 (µg mL^{-1})	E	128	64	32	16	8	4	2	1	0.5	0.25	GC	SC
14 (µg mL^{-1})	F	128	64	32	16	8	4	2	1	0.5	0.25	GC	SC
12 (µg mL^{-1})	G	128	64	32	16	8	4	2	1	0.5	0.25	GC	SC
15 (µg mL^{-1})	H	128	64	32	16	8	4	2	1	0.5	0.25	GC	SC

Figure S22. Antimicrobial testing of leads against *B. subtilis* 3610. Leads were tested alongside DMSO and antibiotic controls for inhibition of bacterial growth. DMSO from the lead compounds was ≤5% (v/v) in wells. Wells in which no bacterial growth was visibly observed are on the left of the red mark and were designated minimal inhibitory concentrations (MICs). "GCs" are growth controls, in which no compound was added, and "SCs" are sterility controls. Plate is representative of duplicate data.

Compound		1	2	3	4	5	6	7	8	9	10	11	12
DMSO (% v/v)	A	80	40	20	10	5	2.5	1.25	0.63	0.31	0.16	GC	SC
Penicillin G (µg mL^{-1})	B	32	16	8	4	2	1	0.5	0.25	0.13	0.06	GC	SC
Chloramphenicol (µg mL^{-1})	C	128	64	32	16	8	4	2	1	0.5	0.25	GC	SC
11 (µg mL^{-1})	D	393	196	98	49	25	12	6	3	2	0.8	GC	SC
12 (µg mL^{-1})	E	293	146	73	37	18	9	5	2	1	0.6	GC	SC
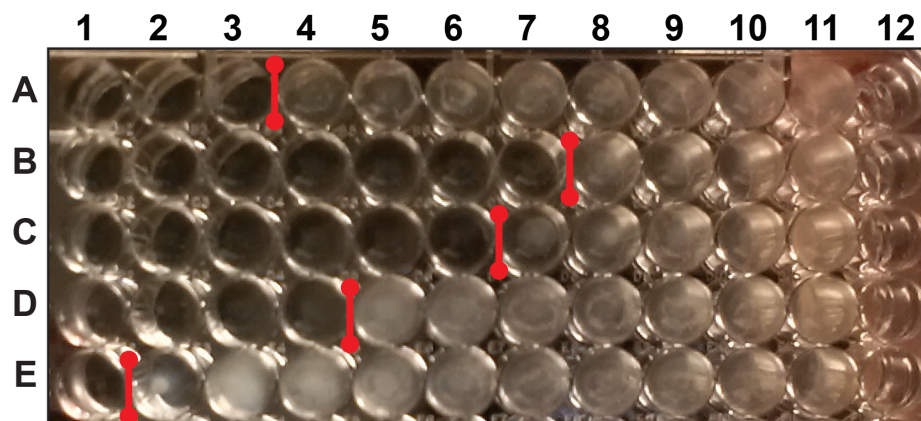
Figure S23. Antimicrobial testing of leads **11** and **12** against *B. subtilis* 3610. Due to the structural similarity between **11** and **12**, higher concentrations of lead were tested to see if **12** would inhibit growth as was observed for **11**. Indeed, growth was inhibited in well E1. DMSO from the lead compounds was ≤5% (v/v) in wells. Wells in which no bacterial growth was visibly observed are on the left of the red mark and were designated MICs. "GCs" are growth controls, in which no compound was added, and "SCs" are sterility controls.

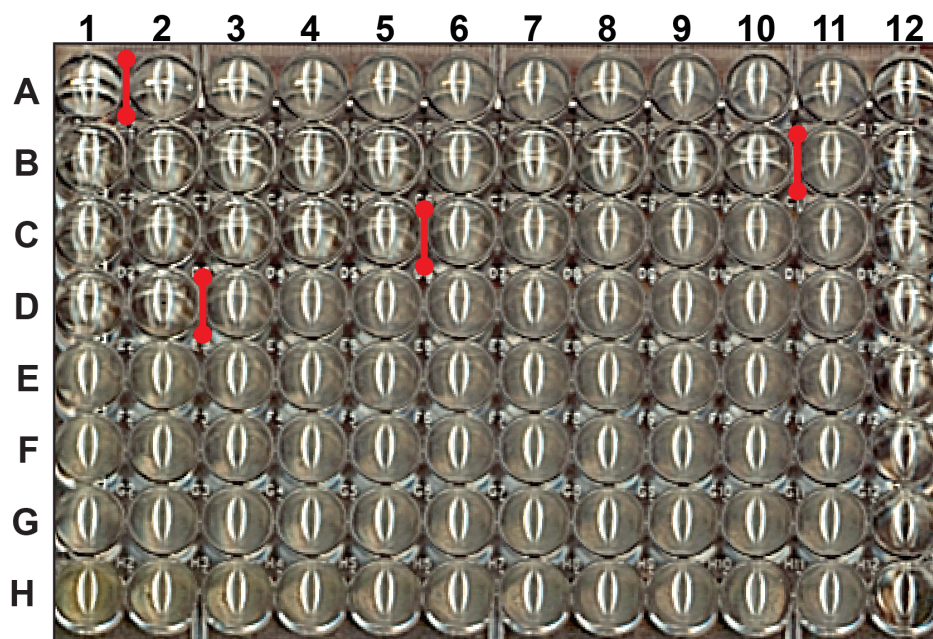| Compound		1	2	3	4	5	6	7	8	9	10	11	12
DMSO (% v/v)	A	20	10	5	2.5	1.25	0.63	0.31	0.16	-	-	GC	SC
Ampicillin (μg mL^{-1})	B	32	16	8	4	2	1	0.5	0.25	0.13	0.06	GC	SC
Chloramphenicol (μg mL^{-1})	C	32	16	8	4	2	1	0.5	0.25	0.13	0.06	GC	SC
11 (μg mL^{-1})	D	128	64	32	16	8	4	2	1	0.5	0.25	GC	SC
13 (μg mL^{-1})	E	128	64	32	16	8	4	2	1	0.5	0.25	GC	SC
14 (μg mL^{-1})	F	128	64	32	16	8	4	2	1	0.5	0.25	GC	SC
12 (μg mL^{-1})	G	128	64	32	16	8	4	2	1	0.5	0.25	GC	SC
15 (μg mL^{-1})	H	128	64	32	16	8	4	2	1	0.5	0.25	GC	SC

Figure S24. Antimicrobial testing of leads against *E. coli* DC2. Leads were tested alongside DMSO and antibiotic controls for inhibition of bacterial growth. DMSO from the lead compounds was ≤5% (v/v) in wells. Wells in which no bacterial growth was visibly observed are on the left of the red mark and were designated MICs. "GCs" are growth controls, in which no compound was added, and "SCs" are sterility controls. Plate is representative of duplicate data.
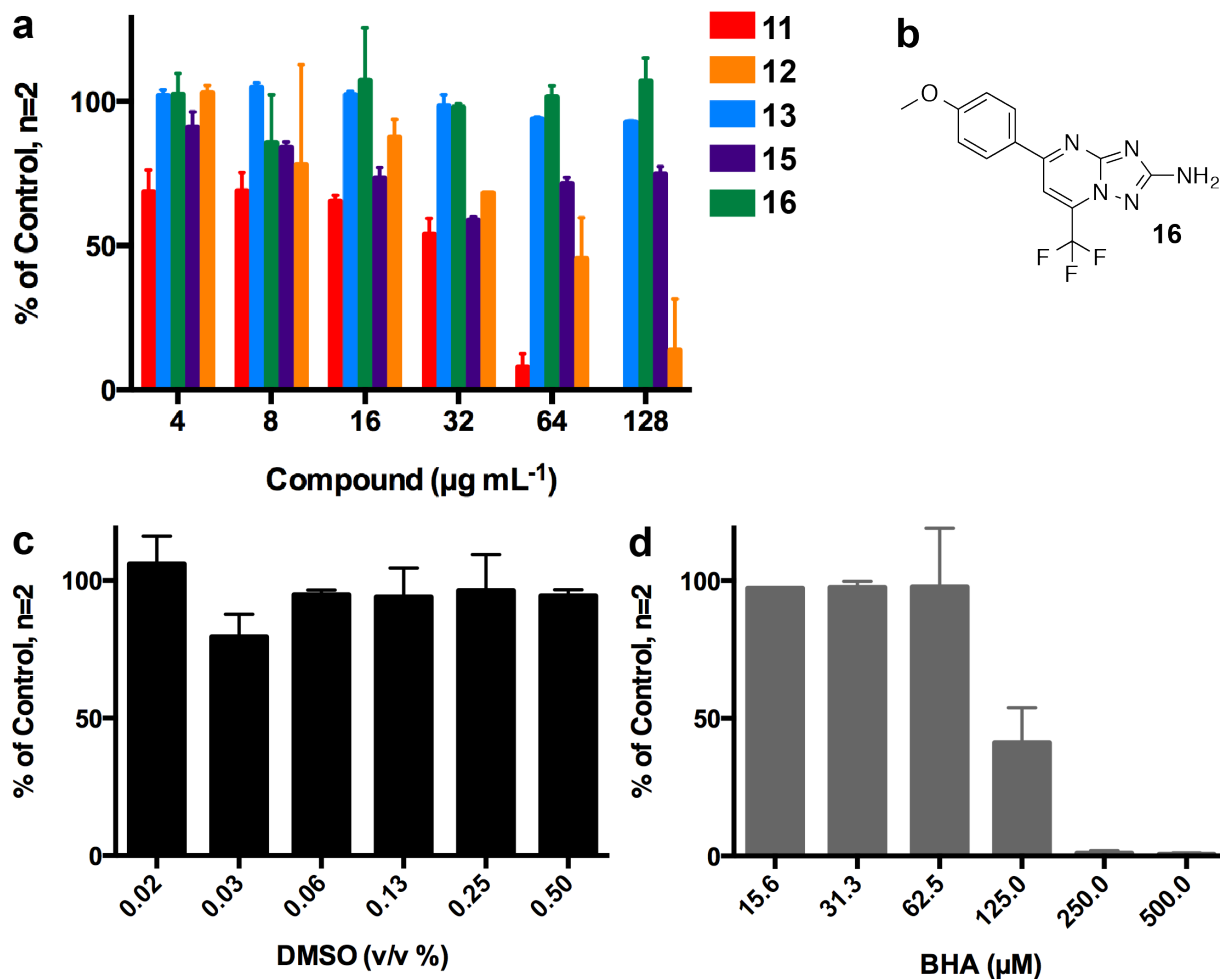
Figure S25. Vero 76 cell cytotoxicity analyses. a) Cytotoxicity assessment of leads with Vero 76 cells. Percent viability was graphed as percent of control (*i.e.*, no compound added). b) An insufficient quantity of compound **14** was available for these experiments. A similar compound, **16**, that is missing a methoxy group at position 3, was examined to provide information about the potential toxicity of this scaffold. c) Vero 76 cell viability with 0.02–0.50% (v/v) DMSO, the concentration of DMSO used in testing lead compounds in part a. d) Butylated hydroxyanisole (BHA) served as a positive control as it was previously shown to have toxic effects on Vero 76 cells. (*7*)
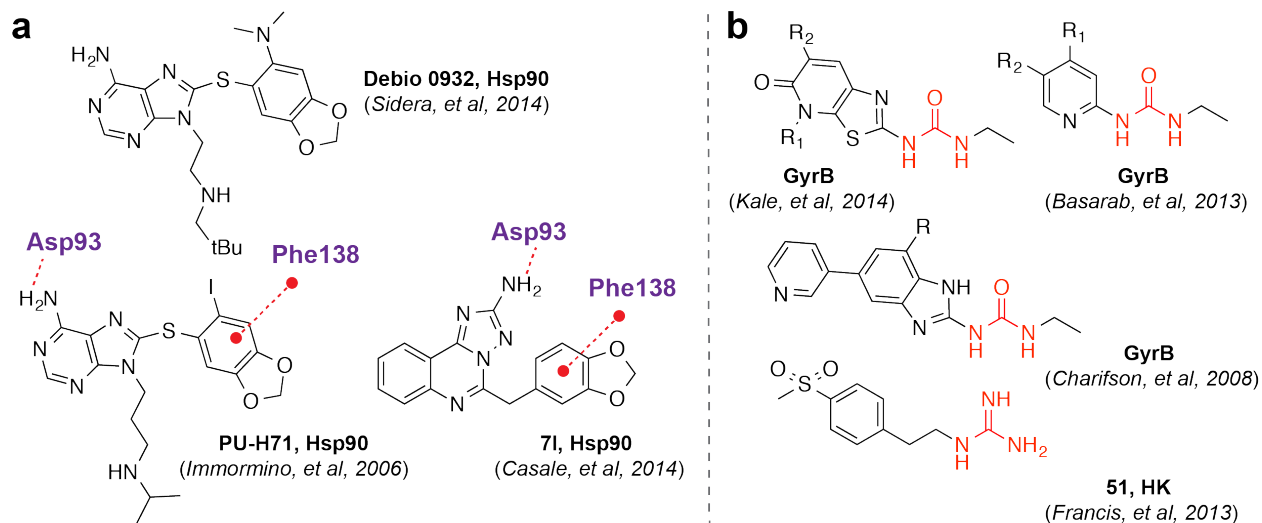
Figure S26. HK inhibitor scaffolds shared with those of GHL proteins. a) Hsp90 inhibitors that resemble the dual-headed purine nature of lead **11,** some of which were shown to bind to residues analogous to those found in HKs, including the invariant Asp.(*8-10*) PDB codes for Hsp90–ligand interactions: 2FWZ (PU-H71) and 4CWP (7I). b) Resembling lead **13**, docking simulations suggest that the urea pharmacophore of GyrB inhibitors and the guanidine group of an active-site targeting HK molecule interact with the Asp in the ATP-binding domain.(*6, 11-13*)

3. Supplementary Table
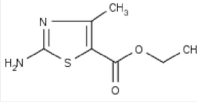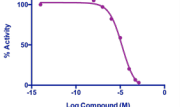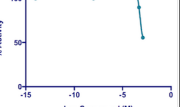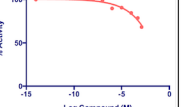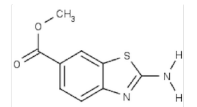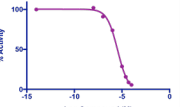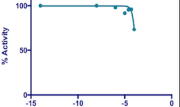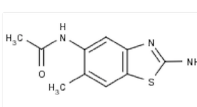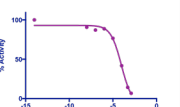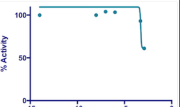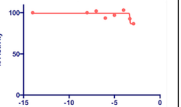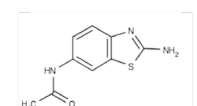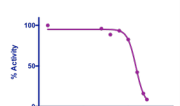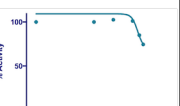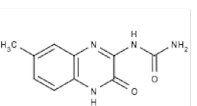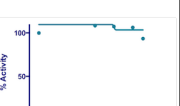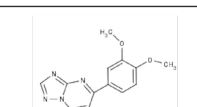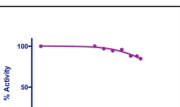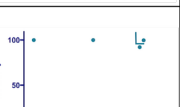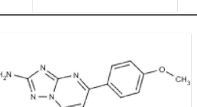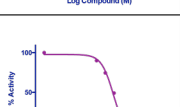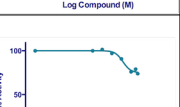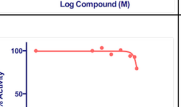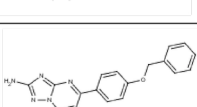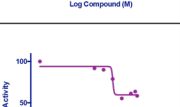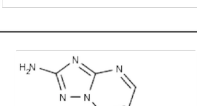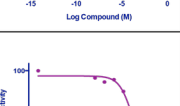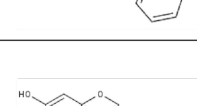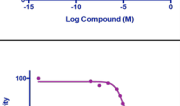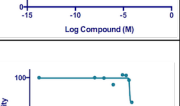
**For Table S1. Summary of 106 Non-Lead Compounds Analyzed in Secondary Screening (pages S23–S33):

[a]"Cut-off" concentration determined in aggregation screening. [b]Data were fit to a four-parameter logistic equation (Equation 1). To acquire estimated IC_{50} values, the bottom of curves were constrained to "0% Activity." [c]On ATP [γ-^{33}P] gels, the final gel band in these preliminary experiments was always of lesser intensity. To further consider compounds for testing, dose-dependent inhibition needed to be observed rather than just at the final data point. Data in Table S1 represents n=1.

Table S1. Summary of 106 Non-Lead Compounds.

	Structure	UM CCG ID / Vendor ID	Cut off (μM)[a]	HK853 Inhibition (B-ATPγS)	HK853 IC$_{50}$ (μM)[b]	VicK Inhibition (ATP [γ-^{33}P])[c]	VicK IC$_{50}$ (μM)[b]	CheA Inhibition (ATP [γ-^{33}P])[c]	CheA IC$_{50}$ (μM)[b]
S1		CCG-118965 ChemDiv 6843-3153	100		8.5				
S2		CCG-118966 ChemDiv 6843-3159	100		11.5				
S3		CCG-118967 ChemDiv 6843-3160	100		12.0				
S4		CCG-121122 ChemDiv 7287-1015	100						
S5		CCG-103937 Vitas-M Laboratory STK373401	100		0.6				
S6		CCG-103302 ChemDiv 0336-0163	100		30.4				
S7		CCG-103030 ChemDiv 0478-0649	100		30.3				
S8		CCG-104503 ChemDiv 1659-1427	1250		42.8				
S9		CCG-109373 ChemDiv 3886-0270	1250		48.0				
S10		CCG-121055 ChemDiv 7286-2215	1250		51.9				

S23

Continued Table S1. Summary of 106 Non-Lead Compounds.

	Structure	UM CCG ID / Vendor ID	Cut off (µM)[a]	HK853 Inhibition (B-ATPγS)	HK853 IC$_{50}$ (µM)[b]	VicK Inhibition (ATP [γ-^{33}P])[c]	VicK IC$_{50}$ (µM)[b]	CheA Inhibition (ATP [γ-^{33}P])[c]	CheA IC$_{50}$ (µM)[b]
S11		CCG-1970 ChemDiv C430-0773	1250		16.2				
S12		CCG-139432 ChemDiv C797-0446	100		3.5				
S13		CCG-107305 Vitas-M Laboratory STL174644	1250		72.6				
S14		CCG-15155 Vitas-M Laboratory STK345876	1250		79.7				
S15		CCG-116733 ChemDiv 6253-0034	1250		154.9				
S16		CCG-121720 ChemDiv 7536-0388	1250						
S17 (*16*)		CCG-121664 ChemDiv 7798-0736	500		0.8				
S18		CCG-120169 ChemDiv 7135-0043	500						
S19		CCG-124396 ChemDiv 8562-00100	1250		61.2				
S20		CCG-38551 ChemDiv 0407-0054	50						

S24

Continued Table S1. Summary of 106 Non-Lead Compounds.

	Structure	UM CCG ID / Vendor ID	Cut off (µM)[a]	HK853 Inhibition (B-ATPγS)	HK853 IC$_{50}$ (µM)[b]	VicK Inhibition (ATP [γ-^{33}P])[c]	VicK IC$_{50}$ (µM)[b]	CheA Inhibition (ATP [γ-^{33}P])[c]	CheA IC$_{50}$ (µM)[b]
S21		CCG-40061 ChemDiv N027-0016	1250		208.5				
S22		CCG-109040 ChemDiv 3770-0086	500		8.3		471.3		
S23		CCG-154218 Vitas-M Laboratory STL070972	500		12.8				
S24		CCG-17978 ChemDiv 3536-0037	1250		22.1				
S25		CCG-125434 ChemDiv C066-5704	500						
S26		CCG-100999 ChemDiv N027-0011	1250		706.5				
S27		CCG-121046 ChemDiv 7283-0987	500						
S28		CCG-122067 ChemDiv 7639-0004	1250						
S29		CCG-122075 ChemDiv 7639-0097	100		17.0				
S30		CCG-146344 ChemDiv D112-0099	500		26.5				

Continued Table S1. Summary of 106 Non-Lead Compounds.

	Structure	UM CCG ID / Vendor ID	Cut off $(\mu M)^a$	HK853 Inhibition (B-ATPγS)	HK853 IC$_{50}$ $(\mu M)^b$	VicK Inhibition (ATP [γ-^{33}P])^c	VicK IC$_{50}$ $(\mu M)^b$	CheA Inhibition (ATP [γ-^{33}P])^c	CheA IC$_{50}$ $(\mu M)^b$
S31		CCG-122077 Vitas-M Laboratory STK856480	100		2.4				
S32		CCG-110901 ChemDiv 4286-0259	100		28.4				
S33		CCG-110902 ChemDiv 4286-0262	100		88.9				
S34		CCG-110903 ChemDiv 4286-0263	1250		91.1				
S35		CCG-121045 ChemDiv 7283-0982	100						
S36		CCG-121047 ChemDiv 7283-0992	100						
S37		CCG-130488 ChemDiv C301-9266	1250		337				
S38		CCG-26899 Vitas-M Laboratory STK617505	1250		14.3				
S39		CCG-107241 ChemDiv 3270-0069	100						
S40		CCG-114935 ChemDiv 5638-0107	500						

S26

Continued Table S1. Summary of 106 Non-Lead Compounds.

	Structure	UM CCG ID / Vendor ID	Cut off (μM)[a]	HK853 Inhibition (B-ATPγS)	HK853 IC$_{50}$ (μM)[b]	VicK Inhibition (ATP [γ-^{33}P])[c]	VicK IC$_{50}$ (μM)[b]	CheA Inhibition (ATP [γ-^{33}P])[c]	CheA IC$_{50}$ (μM)[b]
S41		CCG-24633 ChemDiv 6141-0018	100						
S42		CCG-96497 ChemDiv 7536-0392	1250		27.2				
S43		CCG-121913 Vitas-M Laboratory STL295987	1250		235.1				
S44		CCG-105423 ChemDiv 2284-1590	500		30.8				
S45		CCG-110184 ChemDiv 4100-3971	1250		16.6				
S46		CCG-113790 ChemDiv 5174-3402	500		86.9				
S47		CCG-118215 ChemDiv 6604-0075	1250		446.6				
S48		CCG-120330 ChemDiv 7177-0015	1250						
S49		CCG-124747 ChemDiv 8640-0056	100		63.8				
S50		CCG-125269 ChemDiv C066-4979	100		31.6				

Continued Table S1. Summary of 106 Non-Lead Compounds.

	Structure	UM CCG ID / Vendor ID	Cut off (µM)[a]	HK853 Inhibition (B-ATPγS)	HK853 IC$_{50}$ (µM)[b]	VicK Inhibition (ATP [γ-^{33}P])[c]	VicK IC$_{50}$ (µM)[b]	CheA Inhibition (ATP [γ-^{33}P])[c]	CheA IC$_{50}$ (µM)[b]
S51		CCG-103024 ChemDiv 0345-0104	1250						
S52		CCG-23787 ChemDiv 5820-3404	500						
S53		CCG-122085 Chem-Bridge 7975118	1250		6.4				
S54		CCG-128945 ChemDiv C301-1258	100						
S55		CCG-128946 ChemDiv C301-1259	100						
S56		CCG-129224 ChemDiv C301-3110	100						
S57		CCG-129226 ChemDiv C301-3112	500						
S58		CCG-129508 ChemDiv C301-4530	1250				925.9		
S59		CCG-129601 ChemDiv C301-4755	500						
S60		CCG-129608 ChemDiv C301-4764	500						

S28

Continued Table S1. Summary of 106 Non-Lead Compounds.

	Structure	UM CCG ID / Vendor ID	Cut off (µM)[a]	HK853 Inhibition (B-ATPγS)	HK853 IC$_{50}$ (µM)[b]	VicK Inhibition (ATP [γ-^{33}P])[c]	VicK IC$_{50}$ (µM)[b]	CheA Inhibition (ATP [γ-^{33}P])[c]	CheA IC$_{50}$ (µM)[b]
S61		CCG-66628 ChemDiv C301-4771	1250		1.312				
S62		CCG-66664 ChemDiv C301-4845	100		100.8				
S63		CCG-129961 ChemDiv C301-5833	1250		9.3		735.5		
S64		CCG-161831 ChemDiv E208-0076	500		8.7				
S65		CCG-127065 ChemDiv C200-7706	500						
S66		CCG-127123 ChemDiv C200-7971	100		63.8				
S67		CCG-127124 ChemDiv C200-7972	100		12.2				
S68		CCG-127184 ChemDiv C200-8334	100		6.6				
S69		CCG-127219 ChemDiv C200-8558	100		22.1				
S70		CCG-127220 ChemDiv C200-8559	500						
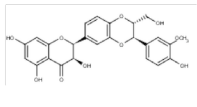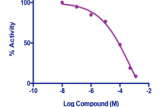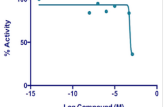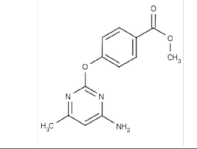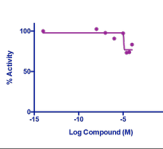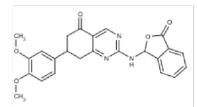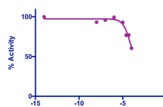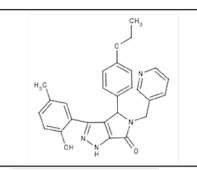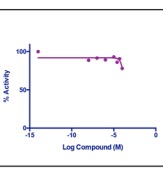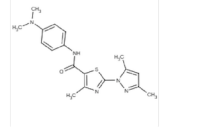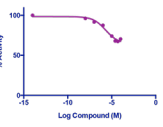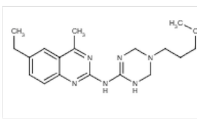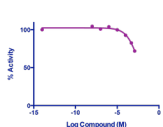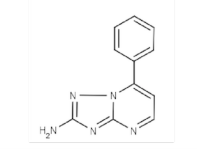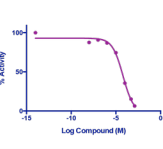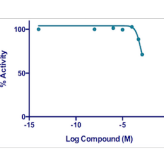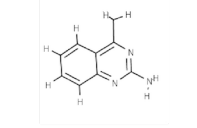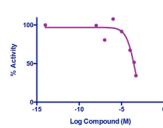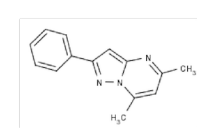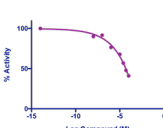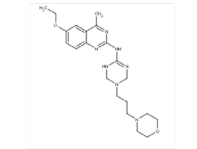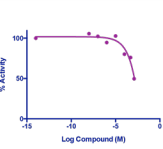
Continued Table S1. Summary of 106 Non-Lead Compounds.

	Structure	UM CCG ID / Vendor ID	Cut off (µM)[a]	HK853 Inhibition (B-ATPγS)	HK853 IC$_{50}$ (µM)[b]	VicK Inhibition (ATP [γ-^{33}P])[c]	VicK IC$_{50}$ (µM)[b]	CheA Inhibition (ATP [γ-^{33}P])[c]	CheA IC$_{50}$ (µM)[b]
S71		CCG-127002 Vitas-M Laboratory STK880124	100						
S72		CCG-141077 ChemDiv C884-2401	100		71.1				
S73		CCG-141079 ChemDiv C884-2422	100						
S74		CCG-141083 ChemDiv C884-2449	100						
S75		CCG-141084 ChemDiv C884-2451	100		42.0				
S76		CCG-100945 ChemDiv 0833-0164	100						
S77		CCG-19474 ChemDiv 4182-0755	100						
S78		CCG-114197 ChemDiv 5348-0038	100						
S79		CCG-120314 ChemDiv 7173-0021	1250		78.8				
S80		CCG-124965 ChemDiv 8640-0596	1250		13.4				
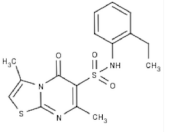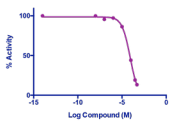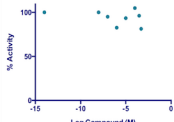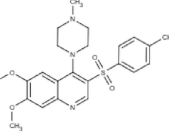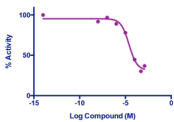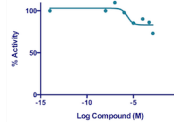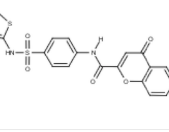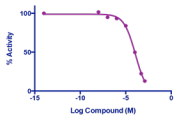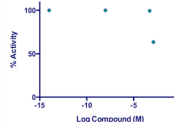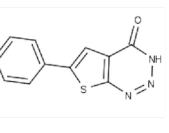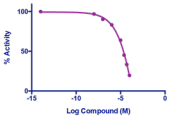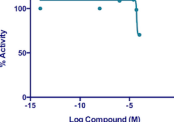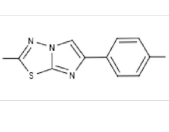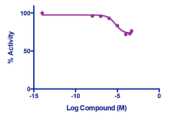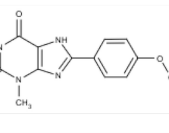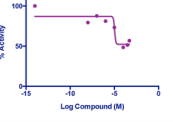
Continued Table S1. Summary of 106 Non-Lead Compounds.

	Structure	UM CCG ID / Vendor ID	Cut off (µM)[a]	HK853 Inhibition (B-ATPγS)	HK853 IC$_{50}$ (µM)[b]	VicK Inhibition (ATP [γ-^{33}P])[c]	VicK IC$_{50}$ (µM)[b]	CheA Inhibition (ATP [γ-^{33}P])[c]	CheA IC$_{50}$ (µM)[b]
S81		CCG-127441 / Vitas-M Laboratory STL145164	500		13.7		606.7		
S82		CCG-122210 / Chem-Bridge 7980846	500		43.9				
S83		CCG-128057 / ChemDiv C248-0005	1250		727.2				
S84		CCG-128064 / ChemDiv C248-0054	1250						
S85		CCG-128072 / ChemDiv C248-0117	1250						
S86		CCG-128075 / ChemDiv C248-0133	1250						
S87		CCG-146881 / ChemDiv D148-0115	500						
S88		CCG-146925 / ChemDiv D148-0474	500						
S89		CCG-148073 / ChemDiv D188-0004	500		242.1				
S90		CCG-148090 / ChemDiv D188-0077	100						

Continued Table S1. Summary of 106 Non-Lead Compounds.

	Structure	UM CCG ID / Vendor ID	Cut off (μM)[a]	HK853 Inhibition (B-ATPγS)	HK853 IC$_{50}$ (μM)[b]	VicK Inhibition (ATP [γ-^{33}P])[c]	VicK IC$_{50}$ (μM)[b]	CheA Inhibition (ATP [γ-^{33}P])[c]	CheA IC$_{50}$ (μM)[b]
S91		CCG-208612 ChemDiv 1363-0007	1250		80.0				
S92		CCG-109375 ChemDiv 3886-0621	100						
S93		CCG-123499 ChemDiv 8249-2138	100						
S94		CCG-146549 ChemDiv D126-0825	100						
S95		CCG-152166 ChemDiv D314-0039	100						
S96		CCG-25565 ChemDiv Y020-0954	1250						
S97		CCG-112943 Vitas-M Laboratory STK709252	1250		55.8				
S98		CCG-37993 Vitas-M Laboratory STK023736	500		288.8				
S99		CCG-112307 ChemDiv 4542-0032	100		52.4				
S100		CCG-121217 ChemDiv 7376-0071	1250						

S32

Continued Table S1. Summary of 106 Non-Lead Compounds.

	Structure	UM CCG ID / Vendor ID	Cut off $(\mu M)^a$	HK853 Inhibition (B-ATPγS)	HK853 IC$_{50}$ $(\mu M)^b$	VicK Inhibition (ATP [γ-^{33}P])^c	VicK IC$_{50}$ $(\mu M)^b$	CheA Inhibition (ATP [γ-^{33}P])^c	CheA IC$_{50}$ $(\mu M)^b$
S101		CCG-129841 ChemDiv C301-5276	500		77.6				
S102		CCG-138104 ChemDiv C769-0917	1250		24.7				
S103		CCG-146186 ChemDiv D103-2285	1250		99.6				
S104		CCG-149823 ChemDiv D243-0117	100		20.9				
S105		CCG-150217 ChemDiv D259-0032	500						
S106		CCG-121003 Vitas-M Laboratory STK575545	500						

4. General Materials and Methods

4A. General reagents

General materials and reagents were obtained from Sigma, Bio-Rad, Millipore, Invitrogen, Fisher, BD (Becton, Dickinson and Company), J.T. Baker, Mallinkrodt, MP Biomedicals, and IBI Scientific except where otherwise noted. BODIPY-FL-ATPγS was purchased from Invitrogen. ATP [γ-^{33}P] was purchased from PerkinElmer. Test compounds were purchased as indicated in Table S1 and Table S2. Milli-Q (MQ) water was used in all experiments, and with the exception of electrophoresis running buffers, all were sterile filtered (0.22 μm). Any value expressed as a percentage is v/v unless noted.

Table S2. Lead compound information: University of Michigan Center for Chemical Genomics (UM CCG) and vendor identifiers.

Compound	UM CCG ID	Vendor	Vendor ID
5	125991	Vitas-M Laboratory	STK944595
6	26901	Vitas-M Laboratory	STL011557
7	26888	ChemDiv	C143-0022
8	125989	Vitas-M Laboratory	STK944594
11	103535	ChemDiv	0717-0926
12	100788	ChemDiv	8012-3510
13	116732	ChemDiv	6253-0032
14	121719	ChemDiv	7536-0387
15	208309	ChemDiv	N027-0009
16	121664	ChemDiv	7798-0736

4B. Protein storage buffer

Buffer for the storage of protein was prepared as 10 mM Tris-HCl, pH 8, 0.1 mM EDTA, 0.5 M NaCl, 12% glycerol, 2 mM DTT.

4C. Determination of protein concentration

Protein stock concentrations were determined by a DC Protein Assay (Bio-Rad) according to the instruction manual and with BSA as a standard. The concentration of at least two dilutions of protein stock were determined and averaged. Where indicated, protein concentration was also determined using a NanoDrop spectrophotometer (Thermo Fisher Scientific) at 280 nm and Beer's Law,

$$A = \varepsilon c \ell \qquad \text{(Equation 3)}$$

where A is absorbance, ε is the protein extinction coefficient ($M^{-1}cm^{-1}$), c is concentration (M), and ℓ is pathlength (cm).

4D. Determination of nucleotide and adenine concentration

After preparing nucleotide working stock solutions in water (or adenine in DMSO), concentrations were confirmed using Beer's Law (Equation 3) by measuring the absorbance on a NanoDrop (adenine extinction coefficient of 15,400 M^{-1} cm^{-1} at 259 nm). For higher concentrations (i.e., millimolar), dilutions (usually 1:100 and 1:1000) were measured and the final concentration averaged. Nucleotide solutions were always prepared fresh.

4E. SDS-PAGE

2X SDS-PAGE sample loading buffer contained 125 mM Tris, pH 6.8, 20% glycerol, 4% SDS (w/v), 5% 2-mercaptoethanol, and 0.2% bromophenol blue (w/v). Tris-glycine stacking gels were prepared with a 10% polyacrylamide resolving gel and 4.5% polyacrylamide

stacking gel. Running parameters were 180 V, 400 mA, and 60 W for 1 h 20 min. SDS-PAGE running buffer was diluted 10-fold from Novex 10X Tris-Glycine SDS Running buffer (Invitrogen) and pre-chilled prior to electrophoresis.

4F. Native-polyacrylamide gel electrophoresis (Native-PAGE)

Native-PAGE sample loading buffer contained 40 mM Tris, pH 7.5, 8% glycerol, and 0.08% bromophenol blue (w/v). Native-PAGE gels were 7.5% polyacrylamide tris-glycine resolving gels. Running parameters were 180 V, 400 mA, and 60 W for 1 h 20 min. The pre-chilled electrophoresis running buffer was 83 mM Tris, pH 9.4, and 33 mM glycine.

4G. Gel fluorescence detection

After SDS-PAGE, gels were washed three times with MQ water. They were scanned on a Typhoon Variable Mode Imager 9210 (Amersham Biosciences) using 526-nm (short-pass filter) detection for BODIPY (λex: 504 nm, λem: 514 nm).

4H. Coomassie staining

Each step was carried out at room temperature (RT) with an orbital shaker. After electrophoresis, gels were washed three times with MQ water and submerged in enough coomassie stain (0.1% (w/v) Coomassie Brilliant Blue R-250, 10% acetic acid, 40% methanol) to cover the gel and incubated for 10 min. Stain was removed, and destain (10% acetic acid, 40% methanol) was added to gel and incubated 30 min. After removing destain, gel was washed in water overnight.

4I. Silver staining

Both SDS-PAGE and native-PAGE gels were silver stained. All steps were carried out at RT with an orbital shaker. After electrophoresis, gels were fixed for 1 h in 20% ethanol, 1% acetic acid. Gels were then washed in 20% ethanol for 10 min. After pre-treating the gel for 1 min in 0.02% (w/v) sodium thiosulfate, gels were washed for 1 min in water. Gels were incubated with 0.1% (w/v) silver nitrate for 20 min and again rinsed for 1 min in water. Developing solution (2% (w/v) sodium carbonate, 0.04% formalin) was incubated with gels for approximately 10 min, or until protein bands were visible, and development was halted with 5% acetic acid for 10 min. Gels were then washed in water.

4J. Gel ATP [γ-^{33}P] detection

Phosphorylation reactions were quenched 1:1 with 2X SDS-PAGE sample loading buffer but were not heated to preserve the phosphohistidine bond. Samples (18 µL) were resolved on 10% SDS-PAGE gels. Afterward, gels were soaked in a solution of 40% methanol, 10% acetic acid, and 8% glycerol for 20 min on an orbital shaker. Sandwiched between filter paper and saran wrap, gels were then dried at 60 °C for 1 h, 70 °C for 1 h, and without heat for 1 h using a gel dryer (Bio-Rad). Gels were exposed to a phosphor screen for 16–20 h and scanned using a Typhoon Variable Mode Imager 9210 under the "phosphorescence" setting.

5. Experimental Methods and Results

5A. ADP-BODIPY (1) synthesis

5A.1. Synthesis of ADP-BODIPY (1)

Adenosine 5′-diphosphate (Sigma Aldrich, sodium salt, 4.4 mg, 9.0 μmol) was dissolved in 1.0 mL of deionized water and added to a round bottom flask that was previously equipped with a magnetic stir bar. After stirring for 1 min, 4,4-difluoro-5,7-dimethyl-4-bora-3a,4a-diaza-s-indacene-3-propionyl ethylenediamine hydrochloride (BODIPY-FL-EDA, Invitrogen, 1.0 mg, 3.0 μmol) was added as a solution in 50 μL H_2O. The reaction mixture was shielded from light using foil and stirred for 10 min after which 1-ethyl-3-(3-dimethylaminopropyl) carbodiimide (EDC, 17 mg, 90 μmol) was added. After 8 h, the reaction mixture was lyophilized and purified using HPLC to yield **1** (1.3 mg, 1.8 μmol, 59%). Purification was performed on an Agilent 1200 HPLC using a reverse phase column (Agilent ZORBAX C_{18}, 5 μm, 250 × 21 mm) equipped with diode array detector (200–600 nm). 0.1M Triethyl ammonium bicarbonate (TEAB) buffer (pH = 8.5) was prepared fresh prior to use. Purification gradients were configured as follows (A = 0.1 M TEAB, B = acetonitrile): 0–5% B (0 to 5 min), 5–15% B (5 to 50 min) using a flow rate of 4 mL min^{-1}. HRMS (m/z): $[M+H]^+$ calcd for $C_{26}H_{34}BF_2N_9O_{10}P_2$ 744.2043; found 744.2068.

5A.2. Freezer stock preparation

ADP-BODIPY (**1**) was dissolved in water to 26 μM, and concentration was confirmed using a Nanodrop Spectrophotometer (absorbance at 504 nm for BODIPY). Probe

solution was aliquoted into amber vials and stored at –20 °C to minimize freeze-thaw cycles.

5B. Protein Production

5B.1.   HK853 overexpression and purification

HK853 (*Thermotoga maritima*; also TM0853) is a membrane-truncated HK that contains a plasmid-encoded His-tag. Under denaturing conditions, HK853 is 32 kDa; under non-denaturing conditions, the dimeric molecular weight is 64 kDa. The molar extinction coefficient is 27,390 $M^{-1}cm^{-1}$. HK853 in the pHis-parallel vector was prepared previously.(*5*)

DNA was transformed into competent BL21(DE3)-pLysS Rosetta *E. coli* cells. Transformed *E. coli* cells were plated overnight on lysogeny broth (LB) agar containing 100 μg mL^{-1} ampicillin (amp) and 34 μg mL^{-1} chloramphenicol (Cm). A single colony was transferred to 100 mL sterile LB media in a 250-mL flask supplemented with antibiotics and incubated at 37 °C overnight at 220 rpm. At OD_{620} of 0.4–0.6, 15 mL was transferred to 1 L sterile LB broth containing antibiotics in 2.8-L baffled flasks. Cultures were grown by shaking at 220 rpm at 37 °C to an OD ~0.6. After equilibrating to 20 °C for three hours, HK853 overexpression was induced with 0.22 mM isopropyl β-D-1-thiogalactopyranoside (IPTG) (Calbiochem) and incubation at 20 °C for 16 h at 220 rpm. Cells were collected by centrifugation at 8000 x g for 20 min, resuspended in 10 mL buffer (25 mM Tris-HCl, pH 8, 500 mM NaCl, 10% glycerol, and 2 mM DTT), and quickly frozen on dry ice for storage at –80 °C.

For purification, each pellet from 1 L of culture was resuspended in a total volume of ~50 mL lysis buffer (25 mM Tris-HCl, pH 8, 500 mM NaCl, 10% glycerol, and 2 mM DTT) containing 20 units Deoxyribonuclease I (Sigma) and four Complete Mini EDTA-free protease inhibitor tablets (Roche). Resuspended cells were lysed by a Branson Sonifier 250 with 1/8-inch tapered microtip (power setting 3.5, duty cycle 30%) for 1 h 20 min on ice. Lysate was centrifuged at 14,000 x g for 40 min at 4 °C. The supernatant was collected and filtered (0.22 µm). Using an AKTApurifier (GE Healthcare) at 4 °C, HK853 was purified from lysate by nickel affinity on a nickel-nitriloacetic acid column (Ni-NTA; Qiagen). Ni-NTA buffer was 25 mM Tris-HCl, pH 8, 500 mM NaCl, 10% glycerol, and 2 mM DTT. An elution gradient of 5 mM imidazole (buffer A) to 1 M imidazole (buffer B) was used to elute His-tagged protein. Eluted HK853 was concentrated for size exclusion chromatography on a HiLoad 16/600 Superdex 75 pg column (GE Healthcare) using 10 mM Tris-HCl, pH 7.6, 0.1 mM EDTA, 0.5 M NaCl, 12% glycerol, and 2 mM DTT. This buffer was also used for storage of protein at −80 °C, in which protein was flash frozen on dry ice/isopropanol. Protein concentration was determined using the DC Protein Assay (Bio-Rad).

5B.2. VicK overexpression and purification

VicK (*Streptococcus pneumoniae*) is a membrane-truncated HK that contains a His-tag. Under denaturing conditions, VicK is 60 kDa. A frozen glycerol stock of BL21(DE3)-pLysS Rosetta *E. coli* cells harboring the VicK plasmid (WalKSpnΔN35 (N)-Sumo) was received as a gift from the laboratory of Malcolm Winkler (Indiana University).(*14*) VicK was overexpressed and purified as previously described.(*5*)

5B.3. CheA/CheW overexpression and purification

CheA (*E. coli*) is the HK of the chemotaxis TCS, and CheW is an adaptor protein of the signaling complex. CheA and CheW are natively cytosolic proteins, and CheA contains a vector-encoded His-tag. Monomeric CheA and CheW are 73 kDa and 18 kDa, respectively. The plasmids pRSF-2 Ek/LIC-CheA and pGEM-T-CheW were gifts from the laboratory of Laura Kiessling (University of Wisconsin-Madison) and were overexpressed and purified as previously described.(*15*)

5C. ADP-BODIPY (1) competition with BODIPY-FL-ATPγS

In addition to the binding curve generated between ADP-BODIPY (**1**) and HK853, we performed a competition experiment with BODIPY-FL-ATPγS (B-ATPγS) to further demonstrate ADP-BODIPY (**1**) binding to the ATP-binding pocket. ADP-BODIPY (**1**) was preincubated with 0.44 µM HK853 for 30 min. B-ATPγS was added and the mixture incubated for 1 h in the dark (25 µL final volume in reaction buffer). The reaction was quenched with 8.6 µL 2X SDS-PAGE sample loading buffer (samples were not heated) prior to transferring 90 ng HK853 into lanes of a 10% stacking gel (Figure S2).

5D. HK853 protein production uniformity

Since many batches of HK853 were produced for screening, they were tested to ensure protein activity was the same. IPTG-induced overexpression of separate batches of HK853 from BL21(DE3)-pLysS Rosetta *E.coli* cells was visualized by lysing cell samples by sonication, mixing lysate 1:1 with 2X SDS-PAGE sample loading buffer, denaturing proteins at 95 °C for 5 min, and resolving proteins by SDS-PAGE and coomassie staining. Batch

activity of purified HK853 was also assessed. In 50-µL reactions, roughly 0.40 µM HK853 from various HK853 batches was reacted with 2 µM B-ATPγS for 1 h at RT in the dark. Reactions were quenched with 17 µL 2X SDS-PAGE sample loading buffer, and HK853 was resolved by SDS-PAGE and in-gel fluorescence detection. Significantly, the amount of protein per lane – as observed in the coomassie-stained image – should be proportional to fluorescence (Figure S27).
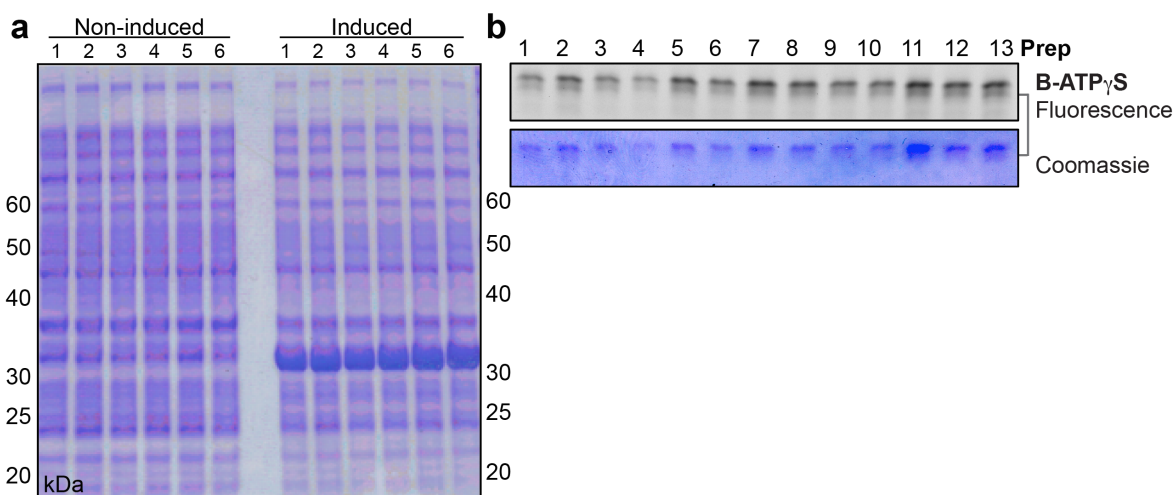
Figure S27. HK853 production uniformity. a) Samples from cultures before and after IPTG-induced HK853 (32 kDa) overexpression. b) Samples from thirteen separate batches of purified HK853 analyzed for activity with B-ATPγS, which is proportional to the amount of protein per lane.

5E. HK853 storage effect on FP

High-throughput screening (HTS) was performed at University of Michigan's Center for Chemical Genomics (UM CCG). Because materials were frozen and shipped on dry ice, we performed FP and activity assays on HK853 stored at different temperatures to ensure the protein binding and/or activity was not compromised. HK853 in storage buffer was prepared

at concentrations similar to those sent to UM CCG (250–300 μM) and incubated at three temperatures overnight: –80 °C (flash frozen), 4 °C, and RT. The next day, protein samples were exchanged into reaction buffer. FP assays with 10 nM ADP-BODIPY (**1**) and 25 μM HK853 (same procedure as discussed in text, n=3) were set up in 96-well plates. The plate was read four times over 24 h to ensure that samples performed similarly (Figure S28A). The same samples were also analyzed for activity with 2μM B-ATPγS (procedure above, n=3) (Figure S28b–c).
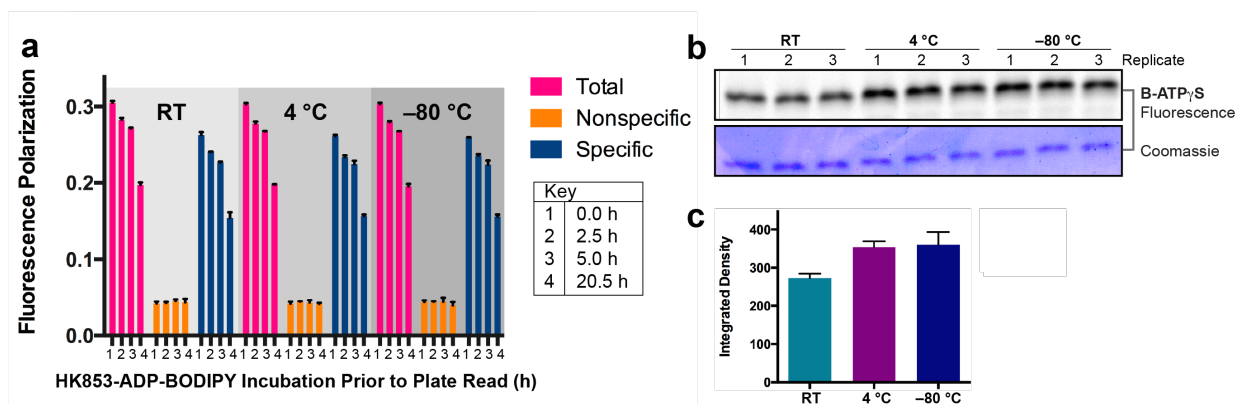
Figure S28. HK853 FP and activity post-storage at various temperatures. a) Total, nonspecific, and specific ADP-BODIPY (**1**) binding to HK853 as measured by FP (n=3) measured at 0, 2.5, 5.0, and 20.5 h after incubation. Specific FP steadily decreased from 0–5.0 h and more significantly decreased over the next 15 h. However, the change in FP over time was constant for all storage conditions. b) B-ATPγS assay showed that HK853 activity was not compromised by the protein freeze-thaw process. c) Raw integrated density values of the fluorescent gel bands in panel b. Samples stored at –80 °C and 4 °C showed higher activity than those at RT. As a result, the flash freezing of HK853 and transport to UM CCG preserves the properties of HK853 important for performance in the HTS.

5F. Determination of ADP-BODIPY (1) concentration for FP competition assays

FP signal should be independent of the intensity of ADP-BODIPY (**1**), but (FIs) should depend on the concentration of fluorescent ligand.(*16*) In 96-well plates, FIs were obtained for 25 μM HK853 mixed with 0–100 nM ADP-BODIPY (**1**) in triplicate. Parallel and perpendicular FIs were plotted as a function of ADP-BODIPY (**1**) to reveal the expected linear relationship (Figure S3b). FP was calculated for the same concentrations of probe and plotted with respect to ADP-BODIPY (**1**) in GraphPad Prism to show that FP remains constant (Figure S3b). We chose to use 10 nM ADP-BODIPY (**1**) in all subsequent assays because it was in the range of limited FP variability. Additionally, using a low concentration ADP-BODIPY (**1**) saved reagent and avoided issues that arise from ligand depletion.

5G. Tolerance of FP assay to Triton X-100

In 96-well plates, ADP inhibition curves were obtained with and without detergent to assess its effect on signal reduction due to molecules that specifically bind HK853. FP was measured for triplicate samples (10 nM ADP-BODIPY (**1**), 25 μM HK853) with and without 0.1% Triton X-100 (Figure S5). No difference in FP or IC_{50} was observed, so Triton X-100 was subsequently used in all displacement assays.

5H. Tolerance of FP assay to DMSO

In 96-well plates, FP was measured (10 nM ADP-BODIPY (**1**), 25 μM HK853) in the presence of 0–10% DMSO (n=3). Another assay was set up to include a saturating concentration of 6 mM ADP to analyze nonspecific binding at increasing concentrations of

DMSO.(*16*) Average FP values were plotted as a function of DMSO in GraphPad Prism (Figure S6).

5I. Determination of statistical values from FP screening data

Z'-factor. The Z'-factor reports on the screening window of an assay, taking both assay signal dynamic range and data variation into consideration.(*17*) The Z'-factor is defined as

$$Z' = 1 - \frac{(3s_{c+} + 3s_{c-})}{|\bar{c}_+ - \bar{c}_-|} \qquad \text{(Equation 4)}$$

where s_{c+} and s_{c-} are the standard deviations of the positive and negative controls, respectively; and $\bar{c}_+$ and $\bar{c}_-$ are the mean values of the positive and negative controls, respectively.

Signal-to-background (S/B). The S/B is the ratio between mean maximum signal and mean minimum signal to describe dynamic range of the signal in an assay.(*17, 18*) The S/B is defined as

$$^S\!/_B = \frac{\bar{c}_-}{\bar{c}_+} \qquad \text{(Equation 5)}$$

where $\bar{c}_-$ is the mean of the maximum FP signal (negative controls), and $\bar{c}_+$ is the mean minimum FP signal (positive controls).

Signal-to-noise (S/N). The S/N describes the strength of the signal within an assay.(*17, 18*) The S/N is defined as the following.

$$S/_N = \frac{\bar{c}_- - \bar{c}_+}{s_{c+}}$$ (Equation 6)

Coefficient of variation (% CV): The % CV is a measure of assay signal dispersion.(*18*) The equation for % CV is as follows and is measured for both positive and negative controls.

$$\% \, CV = \frac{s_c}{\bar{c}} \times 100$$ (Equation 7)

5J. HTS data acquisition, storage, and analysis

Assay miniaturization, primary screening, and confirmation screening were performed at the UM CCG. Data was stored and analyzed in the MScreen database, accessible through an online portal.(*19*)

5K. FP binding assay translation to high-throughput platform

Negative and positive controls were used to confirm the performance of the FP assay in black, flat-bottom, non-binding 384-well plates (Greiner Bio-One, #784900). Assay conditions consisted of 10 nM ADP-BODIPY (**1**) and 25 µM HK853 in reaction buffer (20 µL final volume with 0.01% Triton X-100). High-FP negative controls contained no competitor to represent no inhibition, and low-FP positive controls contained 200 µM ADP to imitate the displacement of the FP probe. A Multidrop dispenser (Thermo Fisher

Scientific, Inc.) delivered HK853, ADP, and ADP-BODIPY (**1**). Mixtures were equilibrated at RT, and FP from the same 384-well plate was measured at 30, 45, 60, and 90 minutes after plating using a PHERAstar (BMG LABTECH) microplate reader (ex: 485 nm; em: 520 nm). Data was unchanged at each time point, ensuring that ADP-BODIPY (**1**) binding to HK853 was at equilibrium and stable over the course of 90 min (Z'-factor 0.87). One plate was prepared without Triton X-100 to confirm that detergent did not alter binding.

5L. Compound libraries at the UM CCG used in screening campaign

Drug Libraries. Collection of drug components, pure natural products with unknown biological properties, and other bioactive compounds (http://www.msdiscovery.com/spectrum.html); specific UM CCG libraries from which compounds were screened were MicroSource Spectrum 2000 and MicroSource 2400

"Focused" Collection. Natural products and compounds from focused libraries for the following targets: autophagy, Wnt pathway, epigenetics, protein kinase, protease, redox, cannabinoid

Biofocus "NCC". Small molecules from the NIH Clinical Collection with a history of use in human clinical trails, including FDA drugs; drug-like molecules with known safety profiles (http://www.nihclinicalcollection.com/)

ChemDiv. Diverse and drug target-focused screening compounds (http://www.chemdiv.com/)

ChemBridge. Diverse and drug target-focused screening compounds (http://www.chembridge.com/); specific UM CCG libraries from which compounds were screened were "ChemBridge 3028" and "ChemBridge 10000"

NCI. Collection from the National Cancer Institute repository of screening compounds

Maybridge Hit Finder ("HF"). Collection of compounds with drug-like diversity (http://www.maybridge.com)

5M. HTS: Pilot screen

The pilot screen using focused compound collections was composed of the following: 2000 small molecules from the MS Spectrum 2000 library, 945 from Focused Collections library, and 446 from the BioFocus NCC library. Assay conditions in 384-well plates were the same as above, and a Biomek FX (Beckman Coulter) with HDR pintool delivered 200 nL test compound to each well (20 μM final compound; 1% DMSO). Thirty-two wells of both negative and positive controls were included on each plate. Samples were equilibrated at RT for 30 min, and FP was measured using a PHERAstar (BMG LABTECH) microplate reader (ex: 485 nm; em: 520 nm). Hits were defined as FP values three standard deviations from the mean of the negative controls. See Table S3 for all screening statistics.

5N. HTS: Primary screening of diverse compounds

5N.1. Transition to 1536-well plates

For higher throughput, a trial screen containing only negative (no competitor) and positive controls (200 μM ADP) was performed to test the feasibility of using 1536-well plates for primary screening. Plates were black, non-binding, with flat bottom (Corning, #3728). Assay conditions were the same as above but in 6 μL volumes. In addition, two separate batches of HK853 were analyzed in this trial screen, and FP values were the same for both protein preparations. There was a slight drift in FP from reading the first well to the last. It was deduced to be a result of temperature increase while the plate was in the reader. This was confirmed by reversing the plate orientation. As a result, quadratic linear regression-based correction was applied to 1536-well plates. MScreen uses row identifier (X), column identifier (Y), and well identifier (W) for deriving the parameters (K, R, C, A and B).

$$CV=Z+M–(K+(X*R)+(Y*C)+((W*W)*A)+(W*B)) \quad \text{(Equation 8)}$$

where CV is the corrected value, Z is the observed signal that needs to be corrected, and M is the mean observed signal value.(*19*) See Table S3 for screening statistics.

5N.2. Primary screening

A total of 49,920 diverse small molecules from the ChemDiv compound collection were screened for the inhibition of ADP-BODIPY (**1**) binding to HK853 in 1536-well plates. Assay conditions were the same as above with 6 μL final volume, and a Sciclone

ALH3000 (Caliper Life Sciences) with V&P Scientific Pin Tool transferred 50 nL test compound to wells (20 µM final, 0.83% DMSO). Each plate included 128 negative and 128 positive controls. See Table S3 for screening statistics.

5O. HTS: Confirmation screen

5O.1. Replicate testing for autofluorescence, quenching, and inhibition

Hit compounds from the primary screen were re-tested in triplicate in 384-well plates for autofluorescence, quenching of the ADP-BODIPY (**1**) probe, and inhibition of probe binding to HK853. Control wells containing ADP-BODIPY (**1**) in buffer were used to adjust gain and establish a threshold for compounds exhibiting high background fluorescence. Compounds were dry spotted with a Mosquito X1 (TTP Labtech) prior to the addition of buffer. Fluorescence was measured in the parallel orientation (ex: 485 nm; em: 520 nm) and compared to ADP-BODIPY (**1**) controls. A threshold of 20,000 relative fluorescence units (RFU) within the parameters of signal acquisition was established, and compounds with fluorescence above it were removed from further testing. ADP-BODIPY (**1**) was then added to all the wells already containing test compounds. The addition of ADP-BODIPY (**1**) resulted in a drastic increase in parallel fluorescence intensity. A threshold of 150,000 RFUs (plate reader maximum of 260,000 RFU) was used to determine quenchers. Compounds in wells that resulted in fluorescence below this threshold were removed from further testing. Lastly, HK853 was added to confirm compound activity in triplicate. See Table S3 for screening statistics.

5O.2. Dose-response curves (DRCs)

Confirmed hits (triplicates with no interfering fluorescence or quenching) were tested for dose-response activity. In 384-well plates, duplicate DRCs were generated from eight concentrations of hit compounds, dry spotted with a Mosquito X1 (TTP Labtech) to range 4–150 μM (final DMSO 1%). DRCs were generated in MScreen according to a four-parameter logistic equation (Equation 1). See Table S3 for screening statistics. Screening hits are summarized in Table S4.

5O.3. Additional DRC compounds

A manual selection of 126 additional compounds from the UM CCG compound collection were included in DRC analysis. These compounds were chosen for one or more of the following reasons:

- Structural similarity to compounds with dose-response activity

- Contained scaffolds or functional groups prevalent in compounds with dose-response activity

- Were active in primary screen but not in DRC (re-test to confirm inactivity)

- Possessed physicochemical properties (*e.g.*, logP, polar surface area) similar to adenosine monophosphate (which was a compound included in the MScreen database so properties could be directly compared)

- Physicochemical properties representative of antibacterials[20]

Table S3. Summary of screening statistics from HTS at UM CCG.

Section	Screen	Z′-factor	S/B	S/N	% CV pos	% CV neg
5M	Primary: Pilot	0.85	6.1	56	9.2	2.6
5N.1.	1536-well plates	0.73	4.5	26	13	4.1
5N.2.	Primary: ChemDiv	0.62	4.7	27	18	5.9
5O.1.	Confirmation	0.73	5.3	38	12	4.9
5O.2.	DRCs	0.77	5.0	37	11	3.8

Table S4. Summary of primary and confirmation screening at UM CCG.

Library	Screened	Hits	Hit Ratio	Confirmed / Dose-Response Activity
MS Spectrum 2000	2000	83	4.15 %	3
Focused Collections	945	49	5.19 %	11
BioFocus NCC	446	50	11.21 %	3
ChemDiv	49920	206	0.41 %	151
ChemBridge 3028*	-	-	-	9
ChemBridge 10000*	-	-	-	1
NCI*	-	-	-	9
Maybridge HF*	-	-	-	1
MS2400*	-	-	-	3

*These were not present in the primary screening. Compounds from these libraries were either manually picked for DRCs or were the same molecules as primary screen hits used to confirm compound activity from different plates/lots.

5P. Compound acquisition and preparation

5P.1. Compound information

Analysis of dose-response curves, previous compound characterization, and availability led to the manual selection of 115 compounds that were purchased from ChemDiv, VitasMLab, or ChemBridge. See Table S2 for compound information.

5P.2. Compound stock solutions

Stock solutions were prepared at 25 mM in DMSO in amber glass vials and agitated and/or sonicated until all compound was visibly dissolved. Stocks were frozen at –20 °C. Prior to use, stocks were briefly set in a 37 °C water bath to facilitate quick thawing.

5Q. Inhibition of HK activity

5Q.1.a. Effect of Triton X-100 on B-ATPγS assay

After aggregation screening, we decided to supplement buffer with 0.1% Triton X-100. To be sure that this would not affect DRC analysis of test compounds, a B-ATPγS assay was used to analyze HK853 ADP DRCs with and without Triton X-100. DRCs were performed as stated in the text, except detergent was premixed into reaction buffer to target a final 0.1% Triton X-100 in one assay (Figure S29).
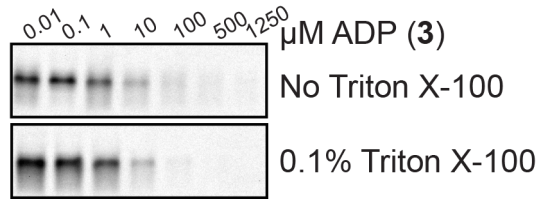
Figure S29. B-ATPγS assays with Triton X-100. Detergent at 0.1% has no effect on DRCs obtained from B-ATPγS assays and was thus added to all B-ATPγS assays.

5Q.3.a. Inhibition of CheA with and without CheW and Triton X-100

Previous studies have shown that CheW drastically increases CheA autophosphorylation in reconstituted signaling complexes.(*15*) To ensure we were testing the appropriate protein(s), we first performed competitive ATP [γ-^{33}P] assays with ADP and 1) CheA alone 2) CheA in complex with CheW, and 3) CheA in complex with CheW in the presence of 0.1% Triton X-100 (Figure S30).
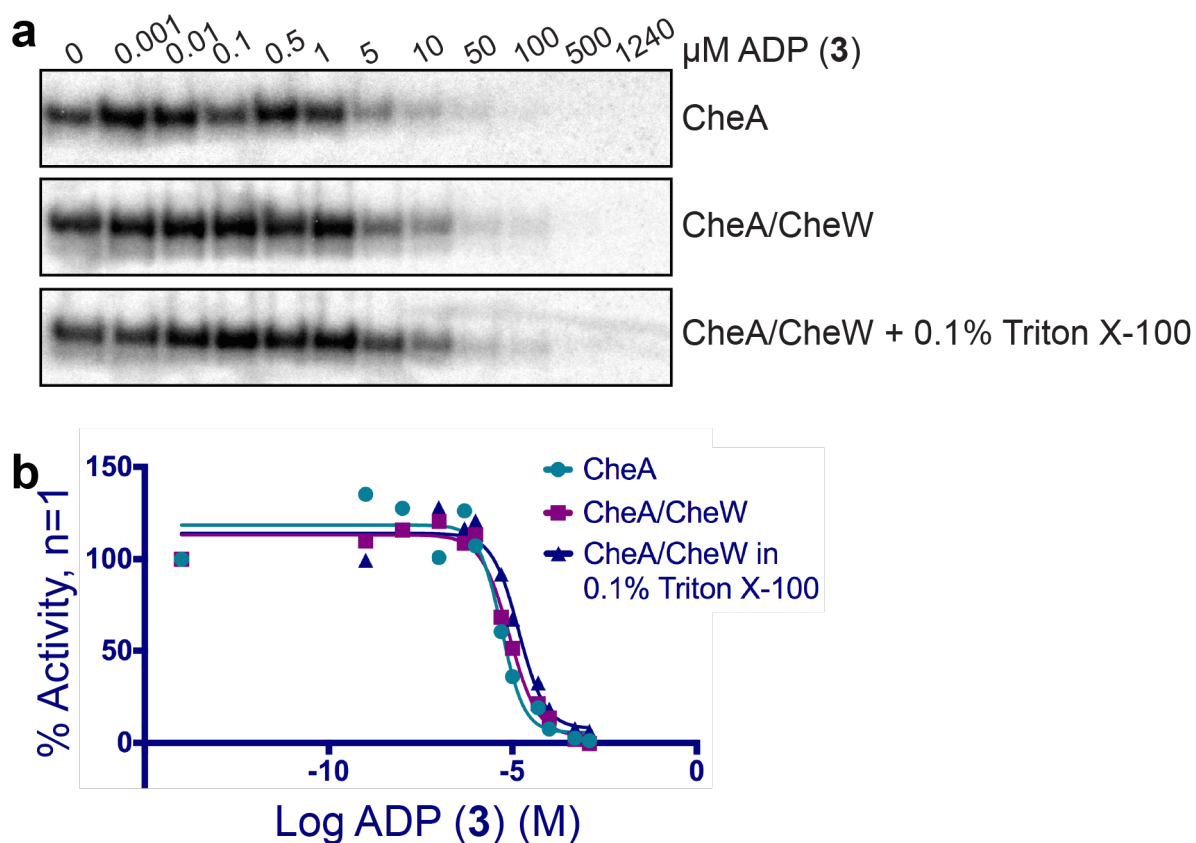
Figure S30. CheA autophosphorylation in the presense of CheW and Triton X-100. The addition of the adaptor protein had minimal effect on CheA autophosphorylation, which is likely because we are not forming the more comprehensive signaling complexes used in previous studies.(*15*) However, in case CheW would affect inhibitor binding, we included it in all CheA analyses. Additionally, Triton X-100 had little effect on the DRC, so it was added to all CheA assays.

5Q.4. Activity confirmation

Competition assays with HK853, VicK, and CheA were repeated for all lead compounds in duplicate to generate 13-point DRCs again analyzed in GraphPad Prism. Aggregation analyses by native-PAGE and silver staining were also repeated using the same 13 concentrations in the presence and absence of Triton X-100.

5Q.5. BSA effect on inhibition

To confirm that compounds were not forming colloidal aggregates and inhibiting HKs nonspecifically, we repeated the HK853 activity assays by competing B-ATPγS with lead compounds **11-15** in the presence of 0.1 mg mL^{-1} BSA.(*21*) These assays were performed in duplicate and did not include Triton X-100.

5R. Cytotoxicity testing

Cytotoxicity of leads **11**-**15** was analyzed with Vero 76 cells (African green monkey kidney epithelial cells; ATCC CRL-1587) using the sodium 2,3,-bis(2-methoxy-4-nitro-5-sulfophenyl)-5-[(phenylamino)-carbonyl]-2H-tetrazolium (XTT) method (XTT Cell Proliferation Assay Kit, ATCC). Vero 76 cells were grown in Dulbecco's modified Eagle's medium (DMEM), 10% fetal bovine serum, 100 U mL^{-1} penicillin, 100 μg mL^{-1} streptomycin, and 2 mM L-glutamine. Cells were maintained at 37 °C in a humidified 5% CO_2 atmosphere, and a solution of 0.25% trypsin, 0.53 mM EDTA was used to detach cells for subculturing. To begin the cytotoxicity assay, 100 μL of a 5.0 x 10^4 cells mL^{-1} suspension was used to seed wells of a 96-well flat-bottom microtiter plate. Vero 76 cells were grown for 24 h in 5% CO_2 at 37 °C and then treated for 24 h with serial dilutions of lead compounds prepared in fresh medium. Wells contained ≤0.5% DMSO. Additionally, DMSO controls, blanks (media only), and growth controls (no compound added) were included; butylated hydroxyanisole (BHA) was used as a positive cytotoxic control.(*7*) To measure cell viability, XTT Cell Proliferation Assay kit instructions were followed. Briefly, activated XTT reagent was incubated with cells in 5% CO_2 at 37 °C for 5 h. Specific absorbance (475 nm) and

nonspecific absorbance (660 nm) was measured on a BioTek Synergy H1M Plate-Reader. Nonspecific and blank absorbance values were subtracted from specific values, which were normalized to a control (i.e., cells with no compound added). Normalized values were plotted in GraphPad Prism with respect to the concentration of compound added in μg mL^{-1} (Figure S26). Concentrations were also converted to molar such that Equation 1 was used to determine the CC_{50} for each lead compound tested, or the concentration at which cell viability was decreased by 50%.

5. References

1.   Dutta, R., and Inouye, M. (2000) GHKL, an emergent ATPase/kinase superfamily, *Trends Biochem. Sci. 25*, 24–28.

2.   Grebe, T. W., and Stock, J. B. (1999) The histidine protein kinase superfamily, *Adv. Microb. Physiol. 41*, 139–227.

3.   Wolanin, P. M., Thomason, P. A., and Stock, J. B. (2002) Histidine protein kinases: Key signal transducers outside the animal kingdom, *Genome Biol. 3*, 3013.1–3013.8.

4.   Xie, W., Dickson, C., Kwiatkowski, W., and Choe, S. (2010) Structure of the cytoplasmic segment of histidine kinase receptor QseC, a key player in bacterial virulence, *Protein Peptide Lett. 17*, 1383–1391.

5.   Wilke, K. E., Francis, S., and Carlson, E. E. (2012) Activity-based probe for histidine kinase signaling, *J. Am. Chem. Soc. 134*, 9150–9153.

6.   Francis, S., Wilke, K. E., Brown, D. E., and Carlson, E. E. (2013) Mechanistic insight into inhibition of two-component system signaling, *Med. Chem. Commun.*, 269–277.

7.   Labrador, V., Fernandez Freire, P., Perez Martin, J. M., and Hazen, M. J. (2007) Cytotoxicity of butylated hydroxyanisole in Vero cells, *Cell Biol. Toxicol. 23*, 189–199.

8.   Casale, E., Amboldi, N., Brasca, M. G., Caronni, D., Colombo, N., Dalvit, C., Felder, E. R., Fogliatto, G., Galvani, A., Isacchi, A., Polucci, P., Riceputi, L., Sola, F., Visco, C., Zuccotto, F., and Casuscelli, F. (2014) Fragment-based hit discovery and structure-based optimization of aminotriazoloquinazolines as novel Hsp90 inhibitors, *Bioorgan. Med. Chem. 22*, 4135–4150.

9. Immormino, R. M., Kang, Y., Choisis, G., and Gewirth, D. T. (2006) Structural and quantum chemical studies of 8-aryl-sulfanyl adenine class Hsp90 inhibitors, *J. Med. Chem. 49*, 4953–4960.

10. Sidera, K., and Patsavoudi, E. (2014) Hsp90 inhibitors: Current development and potential in cancer therapy, *Recent Pat. Anti-Canc. 9*, 1–20.

11. Basarab, G. S., Manchester, J. I., Bist, S., Boriack-Sjodin, P. A., Dangel, B., Illingworth, R., Sherer, B. A., Sriram, S., Uria-Nickelsen, M., and Eakin, A. E. (2013) Fragment-to-hit-to-lead discovery of a novel pyridylurea scaffold of ATP competitive dual targeting type II topoisomerase inhibiting antibacterial agents, *J. Med. Chem. 56*, 8712–8735.

12. Charifson, P. S., Grillot, A.-L., Grossman, T. H., Parsons, J. D., Badia, M., Bellon, S., Deininger, D. D., Drumm, J. E., Gross, C. H., LeTiran, A., Liao, Y., Mani, N., Nicolau, D. P., Perola, E., Ronkin, S., Shannon, D., Swenson, L. L., Tang, Q., Tessier, P. R., Tian, S.-K., Trudeau, M., Wang, T., Wei, Y., Zhang, H., and Stamos, D. (2008) Novel dual-targeting benzimidazole urea inhibitors of DNA gyrase and topoisomerase IV possessing potent antibacterial activity: Intelligent design and evolution through the judicious use of structure-guided design and stucture-activity relationships, *J Med. Chem. 51*, 5243–5263.

13. Kale, R. R., Kale, M. G., Waterson, D., Raichurkar, A., Hameed, S. P., Manjunatha, M. R., Kishore Reddy, B. K., Malolanarasimhan, K., Shinde, V., Koushik, K., Jena, L. K., Menasinakai, S., Humnabadkar, V., Madhavapeddi, P., Basavarajappa, H., Sharma, S., Nandishaiah, R., Mahesh Kumar, K. N., Ganguly, S., Ahuja, V., Gaonkar, S., Naveen Kumar, C. N., Ogg, D., Boriack-Sjodin, P. A., Sambandamurthy, V. K., de Sousa, S. M., and Ghorpade, S. R. (2014) Thiazolopyridone ureas as DNA gyrase B inhibitors:

Optimization of antitubercular activity and efficacy, *Bioorg. Med. Chem. Lett. 24*, 870–879.

14. Gutu, A. D., Wayne, K. J., Sham, L. T., and Winkler, M. E. (2010) Kinetic characterization of the WalRKspn (VicRK) two-component system of *Streptococcus pneumoniae*: Dependence of WalKspn (VicK) phosphatase activity on its PAS domain, *J. Bacteriol. 192*, 2346–2358.

15. Underbakke, E. S., Zhu, Y., and Kiessling, L. L. (2011) Protein footprinting in a complex milieu: Identifying the interaction surfaces of the chemotaxis adaptor protein CheW, *J. Mol. Biol. 409*, 483–495.

16. Auld, D. S., Farmen, M. W., Kahl, S. D., Kriauciunas, A., McKnight, K. L., Montrose, C., and Weidner, J. R. (2012) Receptor binding assays for hts and drug discovery, in *Assay Guidance Manual* (Sittampalam, S., Ed.), Eli Lilly & Company, Indianapolis, IN.

17. Zhang, J.-H., Chung, T. D. Y., and Oldenburg, K. R. (1999) A simple statistical parameter for use in evaluation and validation of high throughput screening assays, *J. Biomolec. Screen. 4*, 67–73.

18. Schürer, S. C., and Tsinoremas, N. F. (2009) Screening informatics, in *A practical guide to assay development and high-throughput screening in drug discovery* (Chen, T., Ed.), pp 233–263, Taylor and Francis.

19. Jacob, R. T., Larsen, M. J., Larsen, S. D., Kirchhoff, P. D., Sherman, D. H., and Neubig, R. R. (2012) MScreen: An integrated compound management and high-throughput screening data storage and analysis system, *J. Biomol. Screen. 17*, 1080–1087.

20. O'Shea, R., and Moser, H. E. (2008) Physicochemical properties of antibacterial compounds: Implications for drug discovery, *J. Med. Chem. 51*, 2871–2878.

21. McGovern, S. L., Caselli, E., Grigorieff, N., and Shoichet, B. K. (2002) A common mechanism underlying promiscuous inhibitors from virtual and high-throughput screening, *J. Med. Chem. 45*, 1712–1722.